Available online at www.sciencedirect.com
ScienceDirect
Acta Materialia 54 (2006) 4953–4975
Acta MATERIALIA
www.actamat-journals.com

Coupling grain boundary motion to shear deformation

John W. Cahn [a], Yuri Mishin [b,*], Akira Suzuki [b]

[a] Materials Science and Engineering Laboratory, National Institute of Standards and Technology, Gaithersburg, MD 20899-8555, USA
[b] Department of Physics and Astronomy, George Mason University, MSN 3F3, 4400 University Drive, Fairfax, VA 22030-4444, USA

Received 23 June 2006; received in revised form 5 August 2006; accepted 7 August 2006
Available online 5 October 2006

Abstract

Molecular dynamics (MD) simulations confirm that normal grain boundary (GB) motion must often be coupled to tangential translation of grains and will then produce shear deformation of the lattice traversed by the GB. Conversely, shear stresses applied to a GB can induce its normal motion. Using [0 0 1] symmetrical tilt GBs in copper as a model, the coupling factor β between the GB motion and grain translations has been calculated by MD simulations over the entire misorientation range and a wide range of temperatures. The coupling factor is multivalued, can be positive or negative, and shows an abrupt switch from one branch to another at a tilt angle of about 35°. At high temperatures the response of high-angle GBs to shear changes from coupling to sliding until coupling disappears. No sliding is observed for low-angle GBs up to near the melting point. A geometric model of coupling proposed in this work predicts the misorientation dependence of β in excellent agreement with MD results and relates the multivalued character of β to the point symmetry of the crystal. Two kinds of low-angle GBs with different dislocations occur when the tilt angle is small and again when it approaches 90°. In these limits, the multiplicity of β is explained by different Burgers vectors of the dislocations. The results of this work are summarized as a temperature–misorientation diagram of mechanical responses of GBs. Unsolved problems and future work in this area are discussed.

Keywords: Grain boundary motion; Shear deformation; Dislocations; Molecular dynamics; Copper

1. Introduction

Grain boundaries (GBs), i.e., interfaces between differently oriented crystallites of the same phase (grains), play a significant role in many processes in materials [1,2]. A unified approach to four fundamental phenomena associated with GBs has recently been formulated [3]:

1. Normal motion (migration), i.e., the process by which a GB moves in its normal direction. The local GB velocity $\mathbf{v}_n$ is parallel to the GB normal vector $\hat{\mathbf{n}}$ and is taken to be positive if it is in the direction of $\hat{\mathbf{n}}$ and negative otherwise. In this process, one grain grows into another and the GB plays the role of the growth and dissolution front.
2. Relative translation of the grains parallel to the GB plane coupled to normal GB motion (Fig. 1(a) and (b)). During this process, the GB shears the material traversed by its motion. The coupled GB motion follows one of several possible geometric relations between $\mathbf{v}_n$ and the relative grain translation velocity $\mathbf{v}_\parallel$ [4,5].
3. Relative rigid-body translation of the grains along the GB by sliding (Fig. 1(c)). In this paper we define and identify GB sliding by grain translation events that are not coupled to normal GB motion.
4. Grain rotation, a process which changes the lattice misorientation across the GB. This process is always accompanied by a relative grain translation along the GB.

In this paper we confine ourselves to cases in which the motions of the grains are parallel to the GB; the case in which the grain translation requires shape accommodation is treated elsewhere [6].

* Corresponding author. Tel.: +1 703 993 3984; fax: +1 703 993 1269.
E-mail address: ymishin@gmu.edu (Y. Mishin).

1359-6454/$30.00
doi:10.1016/j.actamat.2006.08.004

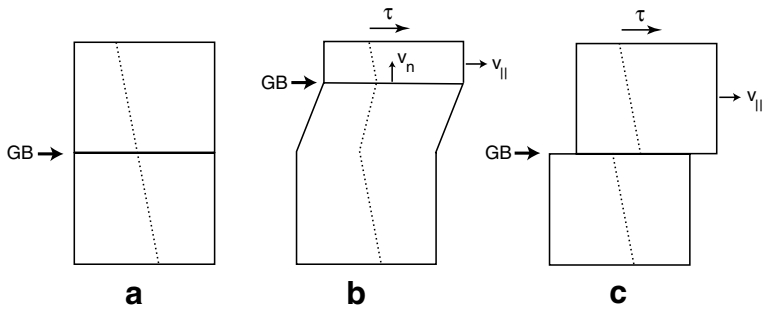

Fig. 1. Two types of response of a planar GB to an applied shear stress τ. (a) Initial bicrystal; (b) GB motion due to coupling; (c) GB sliding. The dotted line crossing the GB represents a set of inert markers embedded in the lattice or any other fiduciary line. v_n and $v_\parallel$ are the velocities of normal GB motion and grain translation, respectively.

The motion of low-angle GBs in Zn bicrystals in response to shear stresses was one of the first observations of coupled GB motion [7,8], and is still a textbook case [9]. Since then, stress-induced motion of tilt GBs with high misorientation angles has been found in Al [10–14] and Zn [15] bicrystals, suggesting that the coupling effect in metals is not limited to low-angle GBs. Coupled GB motion was recently found in cubic zirconia bicrystals [16]. The coupling effect was occasionally observed in first-principles calculations [17–19] and atomistic computer simulations [20–24], but was not clearly identified as a generic phenomenon that must occur in most GBs in both metals and nonmetals.

Tangential translation of grains along a curved GB should give rise to grain rotation [3,6]. In particular, curvature-driven coupled GB motion should almost always be accompanied by grain rotation. Conversely, a shear stress applied along a curved GB not only leads to grain rotation but also creates an additional driving force for the boundary motion towards or even away from the center of curvature. These coupled phenomena can be particularly important in nanocrystalline materials, where grain growth is often accompanied by grain rotation, especially during plastic deformation [23,25–28].

Grain rotation during spontaneous, curvature-driven shrinkage of an enclosed cylindrical grain was studied by atomistic simulations in two [29,30] and three dimensions [31]. The enclosed grain geometry is ideal for revealing the coupling effects as it eliminates all constraints that would otherwise be imposed by triple lines or the free surface. In [31], kinetics of grain shrinkage and rotation were studied for a series of [0 0 1] tilt GBs with tilt angles between $\theta = 5.5°$ and 38.3°. Low-angle grains were observed to rotate to increase θ until about $\theta = 37°$ misorientation.

In this paper we consider a tilt GB under a shear stress τ applied parallel to the GB plane and perpendicular to the tilt axis (Fig. 1). The stress can either induce normal GB motion due to the coupling effect or trigger rigid GB sliding, or both. Assuming additivity of the two effects, the net rate $v_\parallel$ of the relative grain translation can be written as [3]

$$v_\parallel = \beta v_n + v_s(\tau), \tag{1}$$

where β is a coupling factor and $v_s(\tau)$ is the part of $v_\parallel$ which results from sliding under the action of stress τ. Assuming that β is known, Eq. (1) can be applied to determine $v_s(\tau)$.[1]

Without coupling ($\beta = 0$), Eq. (1) reduces to a constitutive law of sliding, $v_\parallel = v_s(\tau)$. The linear law of sliding, $v_s(\tau) \propto \tau$, is adequate at high temperatures but is a poor approximation at low temperatures when sliding does not occur until a threshold stress is approached.

In the absence of sliding ($v_s = 0$) Eq. (1) gives the ideal coupling relation

$$v_\parallel = \beta v_n. \tag{2}$$

Since no driving forces are involved in this relation, it implies that β is a geometric factor which characterizes the shear deformation produced by the GB and which can only depend on crystallographic parameters of the GB [3]. This conclusion was confirmed by previous computer simulations [4,5] and will be further studied in this paper.

While the recognition of the coupling effect reveals new relationships between various seemingly disparate phenomena [3], it also raises new questions:

1. What are the atomic mechanisms of GB motion in the coupling mode? For low-angle symmetrical-tilt GBs (Fig. 2), the mechanism is known to be the collective glide of parallel edge dislocations, forming the GB, in response to the Peach–Koehler forces imposed by the stress τ. The shear deformation of the region traversed by the dislocations leads to a coupled lateral translation of the grains. This simple model [32] predicts that $\beta \approx \theta$, where θ is the tilt angle. In high-angle GBs the dislocations are not resolved. Nevertheless, it was found that coupling still exists with β given by $\beta = 2\tan(\theta/2)$ [4,5]. This implies that the Frank–Bilby equation [1] for the

[1] The following sign convention is assumed in Eq. (1): the GB plane is horizontal, the tilt axis is normal to the paper and **n** points in the up direction, so that v_n is positive if the GB moves up. We take τ to be positive if the force on the upper grain relative to the lower one is to the right, and $v_\parallel$ and v_s to be positive if the upper grain translates to the right relative to the lower one.

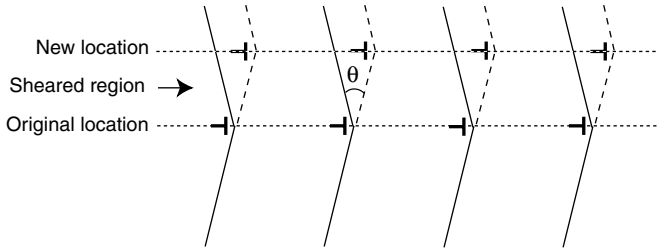

Fig. 2. The dislocation glide mechanism of coupled motion of low-angle symmetrical tilt GBs, and the shear it produces. The solid and dashed lines show selected atomic planes before and after the boundary displacement, respectively. The old and new boundary locations are indicated.

GB dislocation content is applicable to high angles. While simulations [4,5] show good agreement with the Frank–Bilby equation for both small and large angles θ, detailed atomistic mechanisms of coupling in high-angle GBs remain largely unknown.

2. What are the mechanisms of GB sliding? When the GB contains dislocations that can slip in the GB plane, sliding can occur by dislocation glide. Twist GBs do contain such dislocations. The dislocations in the tilt GBs studied in this paper cannot slip in the GB plane and the sliding we observe must happen by some other mechanism. At low temperatures, GB sliding could occur by the nucleation and glide of extrinsic GB dislocations with Burgers vectors parallel to the boundary plane.
3. When and how does the mechanical response of a GB change from coupling to sliding? Is it either coupling or sliding, or can they coexist as postulated in Eq. (1)? Coupling is found to be predominant at relatively low temperatures, whereas sliding is activated at high temperatures and large misorientations. How does the coupling to sliding transition depend on temperature and crystallographic characteristics of the GB?

We attempt to answer these questions with atomistic computer simulations performed on planar $\langle 0\,0\,1\rangle$ symmetrical tilt GBs in Cu over the entire range of tilt angles and a wide range of temperatures. Since the GBs are symmetrical, the grains are oriented to have the same shear moduli parallel to the boundary. Consequently, applied shear stresses do not produce any volume driving forces. The GBs have no curvature and periodic boundary conditions prevent any grain rotation. Thus, in the absence of coupling to shear stresses the GBs can only display random walk by thermal fluctuations. We thus have ideal conditions to study the coupling effect. Since the bicrystal lacks twofold symmetry around the tilt axis, it can interact with shear stresses. Such stresses can only induce GB motion provided this motion produces shear deformation of the bicrystal.

In Section 2, we describe our methodology, which we apply in Sections 3–7 to study GB motion at relatively low temperatures dominated by coupling. We establish the misorientation dependence of β and determine the atomic mechanisms of GB motion. In Section 8, we examine the temperature effect on the GB motion and demonstrate a crossover between coupling and sliding at high temperatures. Our geometric theory of coupling is presented in Sections 9 and 10. Finally, in Section 11 we summarize our findings and outline future work.

2. Methodology

A series of [0 0 1] symmetrical tilt GBs was studied using an embedded-atom potential fit to a large database of experimental and first-principles data for Cu [33]. The potential accurately reproduces a variety of properties of Cu, including the elastic constants, phonon frequencies, thermal expansion, the intrinsic stacking fault energy, the coherent twin boundary energy and others.

A GB was created by constructing two separate crystals with desired crystallographic orientations and joining them along a plane normal to the x-direction (Fig. 3). Periodic boundary conditions were applied in the y- and z-directions parallel to the GB plane, the z-direction being parallel to the tilt axis. Each grain had an approximately cubic shape. Depending on the tilt angle θ and the goal of a particular simulation, the simulation block contained between $(1–5)\times 10^4$ atoms. Molecular dynamics (MD) simulations were performed in the canonical ensemble (Nose–Hoover thermostat) under a fixed volume. To include the effect of thermal expansion, prior to MD simulations the block was expanded uniformly by the lattice thermal expansion factor at the desired temperature T. The thermal expansion factors had been determined previously by zero-pressure Monte Carlo simulations [33]. The MD integration time step was 2 fs and the total time of an MD run was typically a few nanoseconds.

Two types of boundary condition were imposed in the x-direction. In the fixed boundary condition [34], the grains are sandwiched between two slabs in which the atoms are fixed in their perfect-lattice positions relative to one another. The fixed atoms do not participate in MD simulations and only serve to impose interatomic forces on neighboring dynamic atoms. The thickness of each fixed slab is twice the cutoff radius of atomic interactions. The fixed

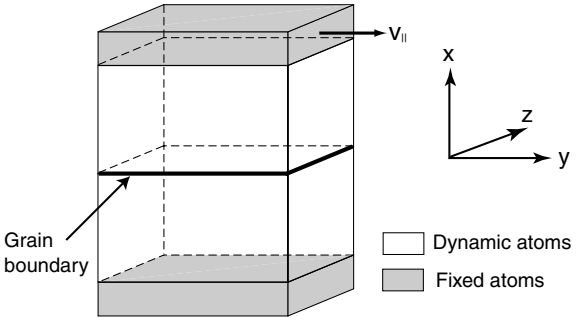

Fig. 3. Geometry of the GB simulation block used in this work. For the fixed boundary condition the atoms in the gray slab are fixed relative to each other and move as a rigid body. The free boundary condition is obtained by replacing all fixed atoms by dynamic atoms. $v_{\parallel}$ is the velocity imposed on the upper fixed slab.

boundary condition restricts spontaneous translations of the grains. Lattice regions adjacent to the GB can still translate relative to each other but such translations are accompanied by elastic deformation of those regions. This boundary condition was used to apply a shear parallel to the GB by moving all fixed atoms of the upper grain with the same constant velocity $v_{\parallel}$, while the lower slab remained fixed.

Most of the simulations reported here were performed under the fixed boundary condition with $v_{\parallel} = 1$ m/s in the y-direction, although some runs were made with smaller velocities down to 10^{-2} m/s in order to probe the strain-rate dependence of the results. This scheme is computationally efficient because it guarantees a significant grain translation over a period of time accessible by MD. We emphasize that this simulation procedure implements shear deformation with a constant rate, whereas the shear stress can vary during the simulation. While constant-stress conditions could be more suitable for testing the observed GB dynamics against theoretical models, they make it difficult to avoid "wasteful" runs in which no interesting events happen if the chosen stress level is too low.

In the free boundary condition, all atoms of the simulation block are made dynamic, so that the grains terminate at free surfaces. MD simulations under this boundary condition are ideal for studying spontaneous GB motion in the coupled regime since the grains are able to translate against each other without any lateral constraints.

The stress tensor averaged over all dynamic atoms was computed using the standard virial expression and was constantly monitored during the MD simulations. The GB position was tracked automatically using the layered structure factor proposed in [35]. The static structure factor $|S(\mathbf{k})|^2$ averaged over atomic layers parallel to the GB plane was calculated for the wave vector $\mathbf{k} = [0, 0, 4\pi/a]$ (a being the lattice parameter of Cu). Since the function $|S(\mathbf{k})|^2(x)$ is almost constant in the grains and has a sharp minimum at the GB, the position of the minimum can be used as a convenient GB locator. Preliminary results of these simulations have been reported in [4,5].

3. Grain boundary structures and coupling modes

The following convention is used to describe the GB crystallography. The tilt axis is parallel to the [0 0 1] direction and normal to the viewer. A symmetrical tilt GB is obtained by taking two identical face-centered cubic (fcc) crystals aligned with the coordinate system and rotating one of them (upper grain) around the tilt axis by $\theta/2$ counterclockwise and the other (lower grain) by $\theta/2$ clockwise. The GB plane is always horizontal and normal to the initially common [1 0 0] direction. Due to the mirrors in the crystal symmetry around the tilt axis, the tilt of each grain by 45° recovers the perfect crystal structure with the (1 1 0) plane horizontal. All distinct GB structures can be observed within the interval $0° < \theta < 90°$. Accordingly, there are two different types of low-angle GBs: when θ is small and when it approaches 90° from below.

Table 1
Characteristics of [0 0 1] symmetrical tilt GBs in Cu studied in this work. γ is the GB energy at 0 K

Boundary	θ (°)	γ(J/m^2)	Mode	β_{MD}	β_{ideal}
Σ101(1 0 1 0)	11.42°	0.684	⟨1 0 0⟩	0.199	0.200
Σ25(7 1 0)	16.26°	0.796	⟨1 0 0⟩	0.287	0.286
Σ37(6 1 0)	18.92°	0.837	⟨1 0 0⟩	0.333	0.333
Σ13(5 1 0)	22.62°	0.878	⟨1 0 0⟩	0.402	0.400
Σ17(4 1 0)	28.07°	0.914	⟨1 0 0⟩	0.497	0.500
Σ53(7 2 0)	31.89°	0.939	⟨1 0 0⟩	0.590	0.571
Σ5(3 1 0)	36.87°	0.905	⟨1 1 0⟩	−1.010	−1.000
Σ5(2 1 0)	53.13°	0.952	⟨1 1 0⟩	−0.667	−0.667
Σ17(5 3 0)	61.93°	0.856	⟨1 1 0⟩	−0.496	−0.500
Σ13(3 2 0)	67.38°	0.790	⟨1 1 0⟩	−0.391	−0.400
Σ37(7 5 0)	71.08°	0.732	⟨1 1 0⟩	−0.338	−0.333
Σ25(4 3 0)	73.74°	0.677	⟨1 1 0⟩	−0.285	−0.286
Σ41(5 4 0)	77.32°	0.595	⟨1 1 0⟩	−0.222	−0.222
Σ61(6 5 0)	79.61°	0.533	⟨1 1 0⟩	−0.195	−0.182

β_{MD} and β_{ideal} are values of the coupling factor β computed by MD simulations at 800 K and predicted by the geometric model, respectively.

Due to the periodic boundary conditions, all GBs studied here had to be coincident site lattice (CSL) boundaries [1]. Each symmetrical CSL GB is uniquely defined by the indices $(hk0)$ of the GB plane[2] and is characterized by a Σ value (reciprocal density of CSL sites). The ground-state structure of each GB was determined by minimizing the total energy of the simulation block with respect to local displacements of dynamic atoms and relative rigid-body translations of the fixed slabs. Table 1 summarizes crystallographic characteristics and 0 K energies of the boundaries studied in this work. They cover tilt angles from 11.42° to 79.61° and Σ values between 5 and 101.

All the GBs contain topologically identical kite-shaped structural units always pointing to the left (Fig. 4). The GBs only differ in the distance separating the kites and their positions relative to the GB plane. The relatively low-angle Σ37(6 1 0) ($\theta = 18.9°$) GB shown in Fig. 4(a) contains an array of dislocations whose cores are formed by the kite units and the Burgers vectors are $\mathbf{b} = [1\,0\,0]$. Likewise, the relatively low-angle Σ41(5 4 0) ($\theta = 77.3°$) GB shown in Fig. 4(d) is composed of $\mathbf{b} = -1/2[1\,1\,0]$ dislocations formed by the kites. The Burgers vectors of the dislocations were determined by the standard Burgers circuit construction.[3] Note that the dislocations in the GBs with θ approaching 0° and 90° have not only different Burgers vectors but also different signs. This can be readily seen by tracing crystal planes which are almost parallel to the GB and noting that the extra half-planes terminating at the dislocations come from the right in Fig. 4(a) and from the left in Fig. 4(d).

[2] Unless otherwise specified, all crystallographic indices used in this work are taken relative to the lattice of the upper grain.

[3] In defining the sign of the Burgers vector we assume that the dislocation line vector is pointing away from the viewer and use the right-hand finish–start (RH/FS) convention [36].

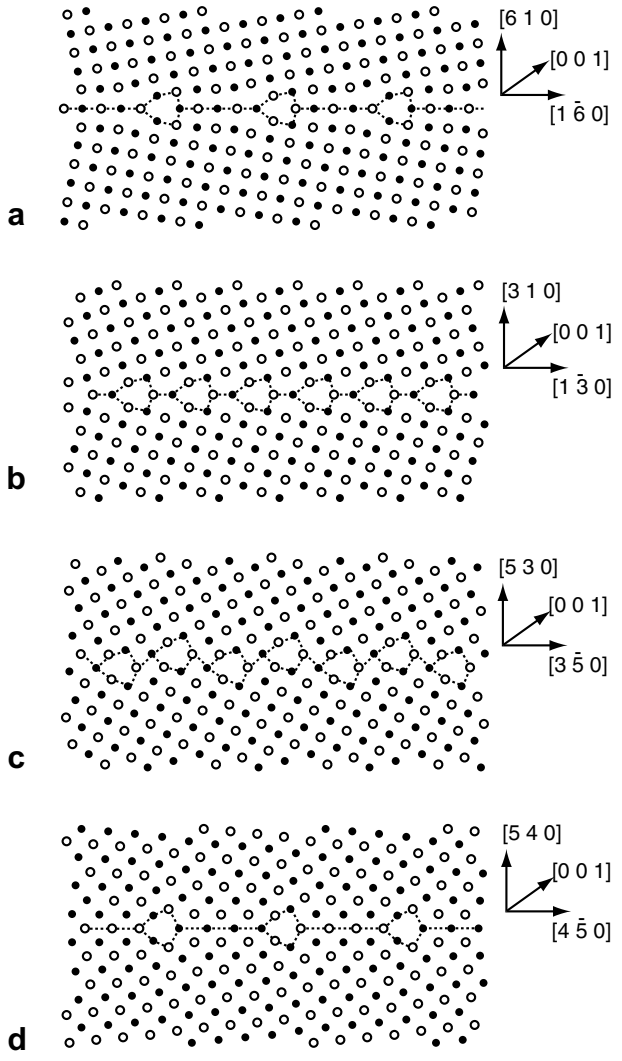

Fig. 4. Atomic structure of selected [001] symmetrical tilt GBs in Cu at 0 K. (a) $\Sigma 37(610)$ ($\theta = 18.9°$); (b) $\Sigma 5(310)$ ($\theta = 36.9°$); (c) $\Sigma 17(530)$ ($\theta = 61.9°$); (d) $\Sigma 41(540)$ ($\theta = 77.3°$). The filled and open circles represent rows of atoms with positions in alternating (002) planes. The structural units and the GB plane are outlined. (a), (b) and (d) are flat boundaries; (c) is an example of a zigzag boundary.

In high-angle GBs, the kites approach each other and form either flat (Fig. 4(b)) or zigzag (Fig. 4(c)) arrays. The zigzag structures are found when $\theta > 45°$ and the indices $(hk0)$ of the GB plane satisfy the condition $h^2 + k^2 = 2\Sigma$. Such boundaries are called centered [37] and for the [001] tilt family occur only if both indices h and k are odd numbers. In such cases the GB plane is parallel to a {110} plane of the CSL of the bicrystal. The non-centered (flat) boundaries are parallel to a {100} CSL plane and satisfy the condition $h^2 + k^2 = \Sigma$.

It has been shown [5] that the 4mm crystal symmetry around the ⟨100⟩ axis gives rise to two branches of the misorientation dependence of β. One branch, termed ⟨100⟩ according to the slip direction of GB dislocations, originates from the coupled motion of low-angle GBs with $\theta \to 0$ and is described by the equation

$$\beta_{\langle 100\rangle} = 2\tan\left(\frac{\theta}{2}\right). \tag{3}$$

The other branch termed ⟨110⟩ corresponds to coupled motion of low-angle GBs with $\theta \to 90°$ and is given by

$$\beta_{\langle 110\rangle} = -2\tan\left(\frac{\pi}{4} - \frac{\theta}{2}\right). \tag{4}$$

These equations are derived from geometric models of coupling which will be discussed later (Section 9). Here we only introduce these equations for future references.

4. Stress-induced boundary motion at medium temperatures

Shear was applied to all GBs by shifting the fixed atoms of the upper grain to the right with a constant velocity $v_{\|}$. At temperatures above ~500 K and up to at least 800 K, all GBs were observed to move either up or down with a constant average velocity v_n. The situation at lower and higher temperatures can be different and will be discussed separately (Sections 5 and 8). The stress-induced GB motion is illustrated in Fig. 5, which shows that v_n can be either positive or negative, depending on θ. Note the uniform shear deformation of the initially rectangular shape of the simulation block in the region traversed by the GB.[4] This shear is a signature of the coupled GB motion and can be contrasted to rigid sliding along the GB in which the block would be simply cut in two halves along the GB plane (cf. Fig. 1). The lattice regions left behind the moving GBs were carefully examined for vacancies or any other lattice defects. No defect generation was found in any simulations reported in this work. It was also found that by reversing the direction of the grain translation each GB could be moved in the opposite direction with exactly the same v_n.

Fig. 6 shows typical plots of the normal GB displacement versus time at 800 K. The average GB velocities v_n were determined by mean-squared linear fits to such plots. Note that all GBs with $\theta < 36.9°$ move up while the rest of the GBs move down, indicating that the coupling effect is discontinuous and changes sign.

Some of the GBs clearly reveal an incremental, stop-and-go, character of motion while others appear to move in a more stochastic manner at this temperature. At lower temperatures, all GBs move by a stop-and-go mechanism, each with its own increment of the normal displacement H and the associated grain translation S. The relation of H and S to GB structure will be discussed later (Sections 9.4 and 9.5). Incremental motion of GBs has been observed experimentally [38].

[4] In typical MD simulations with periodic boundary conditions the initial shape of the simulation block is preserved by mapping atoms back into the block if they attempt to leave it. While this scheme has computational advantages, it masks the deformation and motion of the grains and is not suitable for studying GB coupling or sliding. In our simulations the atoms are not mapped back into the initial block.

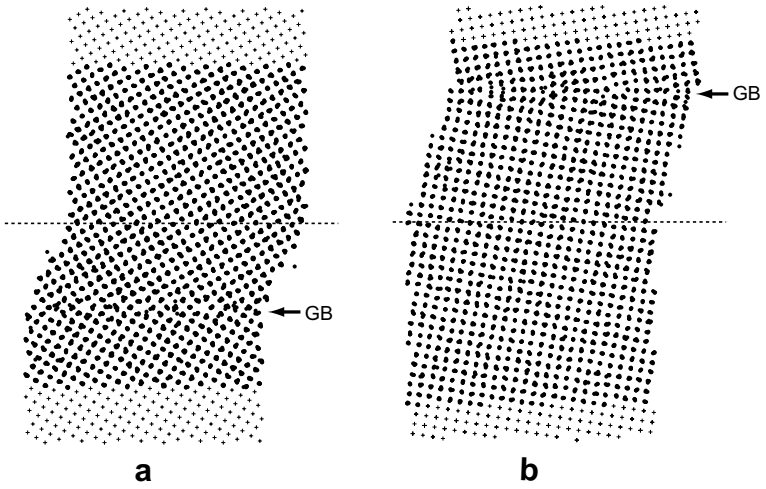

Fig. 5. Typical snapshots of MD simulations of stress-induced motion of the (a) Σ17(530) ($\theta = 61.93°$) and (b) Σ37(610) ($\theta = 18.92°$) GBs at 800 K under the same shear direction. The circles and crosses show projections of dynamic and fixed atoms, respectively. The initial position of the GB is shown by a horizontal dotted line and the final position is indicated by an arrow. The shear rate is 1 m/s and the MD time is 1.2 ns. The different directions of the GB motion point to different signs of the coupling factor β.

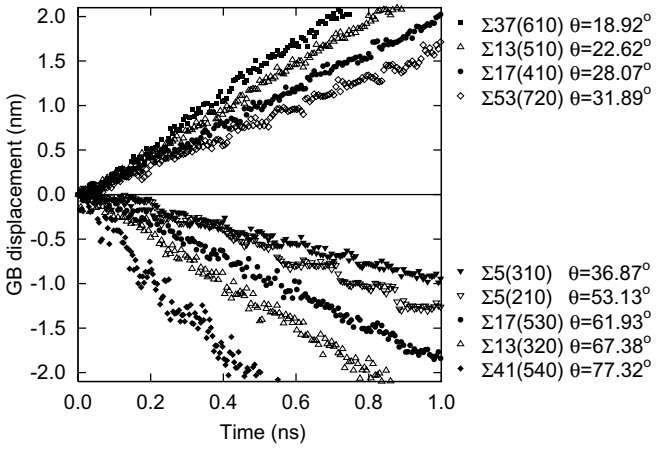

Fig. 6. GB displacement versus time during MD simulations at 800 K under a shear parallel to the GB plane and normal to the tilt axis. The shear rate is 1 m/s.

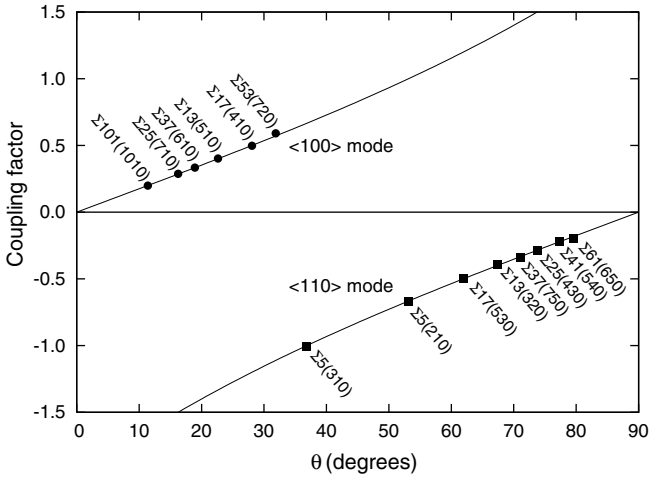

Fig. 7. The coupling factor β obtained by MD simulations at 800 K as a function of the tilt angle θ. The lines represent two branches of β predicted by the geometric model of coupling.

The coupling factor $\beta = v_{\parallel}/v_{\mathrm{n}}$ was calculated from these simulations. The results obtained at 800 K with $v_{\parallel} = 1$ m/s are listed in Table 1 and the observed misorientation dependence of β is plotted as points in Fig. 7. The two curves shown in this figure were calculated from Eqs. (3) and (4). All β values obtained by the MD simulations fall on these two curves. Note the sudden switch between the curves between the Σ53(720) ($\theta = 31.9°$) and Σ5(310) ($\theta = 36.9°$) misorientations. This switch is accompanied by a change of sign of β from $\beta > 0$ at $\theta \leqslant 31.9°$ to $\beta < 0$ at $\theta \geqslant 36.9°$. Calculations of β at all temperatures between 500 and 800 K and with $v_{\parallel}$ between 0.01 and 1 m/s gave virtually identical results, confirming that β behaves as a geometric factor. Such agreement between the observed and geometrically predicted β values will be called "perfect coupling". The angle at which β changes sign does not depend on temperature within the 500–800 K range as indicated in Fig. 8.

Fig. 7 displays the central result of our work, which will be discussed and interpreted in subsequent sections of this paper: not only does the perfect coupling exist for both low- and high-angle GBs, but also the misorientation dependence of the coupling factor derived for low-angle GBs continues to be perfectly accurate for all high-angle misorientations. The observation of the discontinuous behavior of β is another important result of the simulations.

Typical shear stress behavior during the coupled GB motion is illustrated in Fig. 9. The stress increases almost linearly due to elastic deformation of the material until a critical value is reached at which the boundary makes a rapid move to a new position a distance H away from the previous one. The stress drops to a value which depends on the simulation block size in the normal direction and can be either positive or negative. This drop of stress is

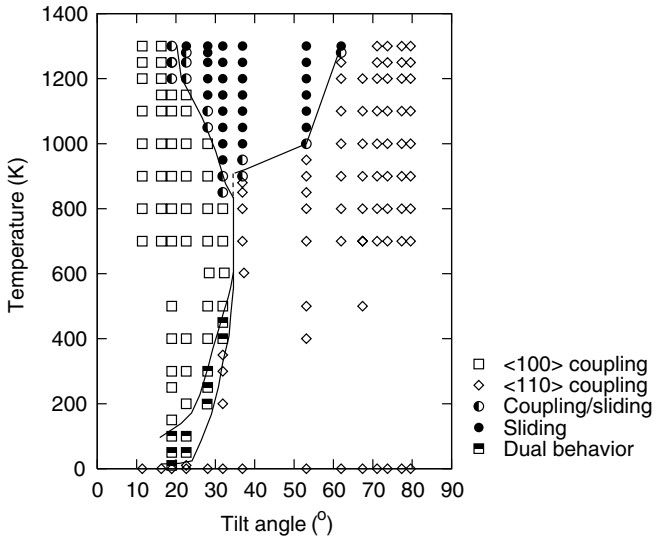

Fig. 8. Diagram of mechanical responses to shear of [0 0 1] symmetrical tilt GBs in Cu.

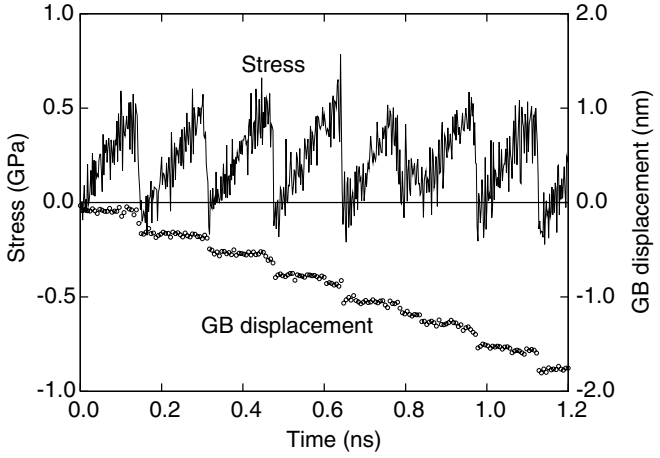

Fig. 9. Time dependencies of the shear stress and GB displacement during the coupled motion of the Σ5(2 1 0) GB at 700 K with $v_{\|} = 1$ m/s, illustrating the stick–slip character of GB migration.

followed by a new increase until the next peak, and the process repeats. Thus, the shear stress displays a very clear stick–slip behavior which is well known in sliding friction [39,40]. As expected, the scatter in the stress peak heights and positions increases with temperature. While the average values of H and S typically remain nearly constant and are determined by the GB geometry,[5] the average height of the stress peak decreases with increasing temperature or decreasing $v_{\|}$.

Examination of MD snapshots shows that GB self-diffusion took place during some of the coupling simulations at the high end of the temperature range. As a crude estimate of the range of diffusional motion, one can compare the diffusion length over the time when an atom resides within the moving GB, $[D\delta/v_n]^{1/2}$, with interatomic distance (δ is the GB width). For example, at 800 K a typical value of $D\delta$ in Σ5 Cu GBs calculated with the same EAM potential is about 2.5×10^{-20} m^2/s [41]. Taking one of our GB velocities $v_n \approx 0.01$ m/s, we obtain $[D\delta/v_n]^{1/2} \approx 1.2 \times 10^{-9}$ m, which is about four times the interatomic distance 3×10^{-10} m. At higher temperatures the amount of GB diffusion increases. This estimate confirms that GB diffusion can occur and does not seem to affect perfect coupling. This is consistent with the notion that coupling is associated with a geometrical correspondence between lattice sites but not necessarily between individual atoms.

5. Stress-induced boundary motion at low temperatures

Coupled GB motion continues to exist at low temperatures, where it is strongly dominated by stick–slip behavior of the stress. Under such conditions, the frequently assumed linear relation between GB velocity and stress is not an adequate approximation. Instead, we postulate that there is a critical value of the applied shear stress, τ_{ci}, needed to activate a particular coupling mode $i = \langle 1\,0\,0\rangle$ or $\langle 1\,1\,0\rangle$. The GB does not move unless $\tau > \min(\tau_{c\langle 1\,0\,0\rangle}, \tau_{c\langle 1\,1\,0\rangle})$.

For low-angle GBs we expect that τ_{ci} satisfies the relation

$$\tau_{ci} S_i(\theta) = \sigma_{ci}(\theta), \tag{5}$$

where $S_i(\theta)$ is the Schmid factor for the dislocation slip plane and slip direction corresponding to mode i and $\sigma_{ci}(\theta)$ is the respective critical resolved shear stress. The resolved (glide) shear stress $\tau S_i(\theta)$ is proportional to the glide component of the Peach–Koehler force acting on the dislocations. Relation (5) expresses the postulated Schmid law, which ignores all non-glide components of the stress and predicts that the coupling mode with the smaller ratio $\sigma_{ci}(\theta)/S_i(\theta)$ must prevail. At low enough temperatures, σ_{ci} can be identified with the Peierls–Nabarro stress for the collective glide of the array of parallel straight dislocations, which can be different from the Peierls–Nabarro stress of an isolated dislocation. Note that the GB dislocations considered here can have unusual Burgers vectors and glide on unusual slip planes. At higher temperatures, the dislocations can move by kink-pair formation and extension and the meaning of σ_{ci} becomes more complex.

For the [0 0 1] tilt GBs we have $S_i(\theta) = \cos\theta$ for the $\langle 1\,0\,0\rangle$ mode and $\cos(\pi/2 - \theta)$ for the $\langle 1\,1\,0\rangle$ mode. The two Schmid factors are equal when $\theta = \pi/4$. Assuming that Eq. (5) continues to hold for high-angle boundaries, and recalling that the change of the coupling mode occurs at $\theta < \pi/4$ (Fig. 7), we conclude that σ_{ci} for the $\langle 1\,0\,0\rangle$ mode is larger than for the $\langle 1\,1\,0\rangle$ mode in this misorientation range. We will be examining σ_{ci} in both modes in more detail later (Section 10).

As shown in Fig. 8, as the temperature drops, the θ range of the $\langle 1\,1\,0\rangle$ mode expands and at $T \to 0$ may cover

[5] See Fig. 10 for an exception.

all angles studied, while the range of the ⟨100⟩ mode shrinks to small θ. There is an overlap area, which we term "dual behavior", in which both modes are observed at the same θ. In all cases of dual behavior, the GB begins to move in the ⟨110⟩ mode but later switches to the ⟨100⟩ mode and remains in it until the end of the simulation. This observation of spontaneous reversal of coupled GB motion shows that both coupling modes can be implemented in the same boundary at the same temperature. This dual behavior is only observed within a relatively narrow (~100 K) temperature range specific to each GB. The time of the switch between the coupling modes depends on the temperature, θ and $v_{\|}$. At temperatures above the dual area in Fig. 8, the GB makes its first movement in the ⟨100⟩ mode and the ⟨110⟩ mode is never observed.

An example of dual behavior is given in Fig. 10. The average slopes of the displacement–time curves in the beginning of the run and after the reversal give β values which are in good agreement with Eqs. (4) and (3), respectively. Thus, the reversal signifies an abrupt switch from one branch of the ideal coupling relation $\beta(\theta)$ to another at the same θ. This clearly demonstrates that β is a multivalued function of θ. Note that after the initial period of time comprising three stick–slip events the critical stress drops and the increments H and S of the GB motion change. The switch to the ⟨100⟩ mode after 1.5 ns is associated with another, although smaller, decrease of the critical stress. The time-dependent critical stress reflects the change in the GB migration mechanism as well as possible changes in the boundary structure.

For each boundary there is a temperature below which only ⟨110⟩ motion is observed; a switch to the ⟨100⟩ mode never occurs during the simulation times available to us. This allowed us to determine $\beta_{\langle 110\rangle}$ for all GBs studied here by choosing low enough temperatures. The values thus obtained lie exactly on the theoretically predicted ⟨110⟩ branch of $\beta(\theta)$, given by Eq. (4), over the entire misorientation range we studied. On the other hand, we were unable to observe the ⟨100⟩ mode of coupling below a certain temperature which depends on θ. This limited our $\beta_{\langle 100\rangle}$ calculations to relatively high temperatures and the angular range $\theta \lesssim 35°$ (Fig. 8), where $\beta_{\langle 100\rangle}$ was found to be independent of temperature.

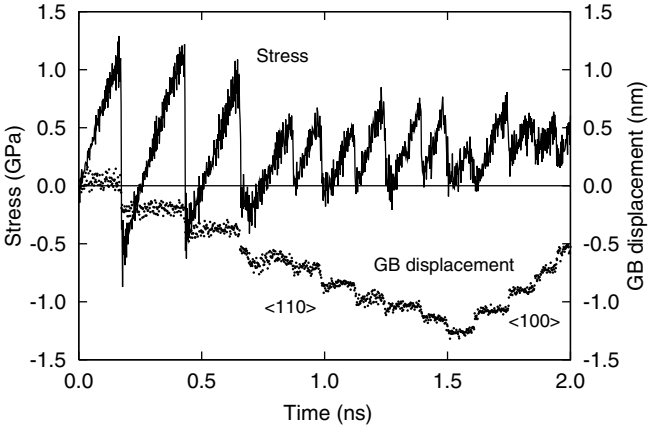

Fig. 10. Shear stress and GB displacement as functions of time for the Σ53(720) GB at 400 K. The GB switches from the ⟨110⟩ to the ⟨100⟩ mode of coupling after 1.5 ns. The peak stress and the time interval between GB displacements change after 0.7 ns.

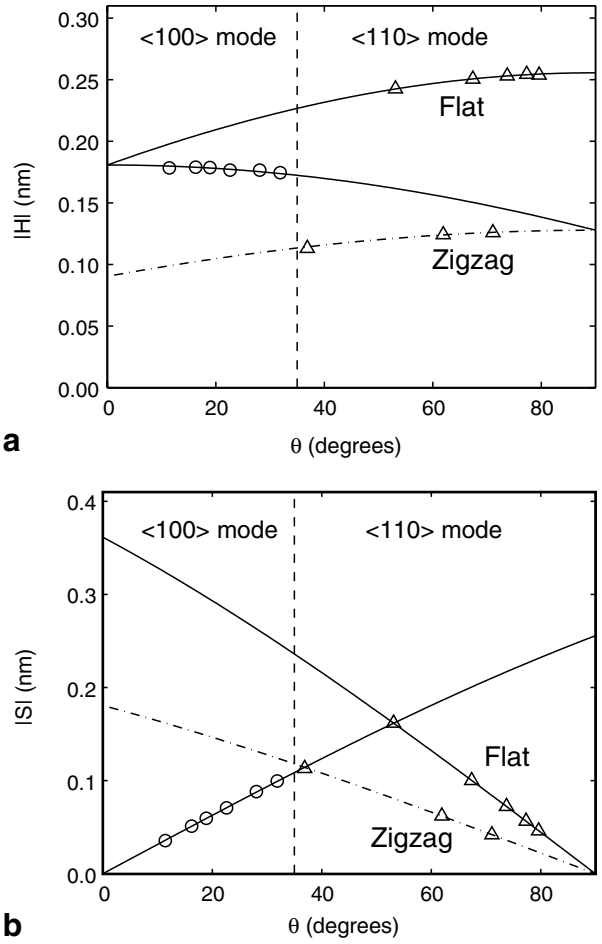

Fig. 11. Absolute values of the increments of (a) normal GB displacement H and (b) tangential grain translation S, during coupled motion of [001] symmetrical tilt GBs. The circles and triangles represent results of atomistic simulations for the ⟨100⟩ and ⟨110⟩ modes, respectively. The solid lines are obtained from Eqs. (9)–(15), the dash-dotted line corresponds to a half of the H and S values for the ⟨110⟩ mode. The vertical dashed line indicates the angle of switch between the coupling modes at 500–800 K.

Fig. 11 displays the θ dependence of H and S determined from MD snapshots under ideal coupling and stick–slip conditions. There is one branch for the ⟨100⟩ mode and two branches for the ⟨110⟩ mode. Their interpretation will be discussed in Sections 9.4 and 9.5.

6. Spontaneous boundary motion

Some of the GBs were observed to move during the MD simulations as a result of thermal fluctuations even without applied shear. This spontaneous GB motion was especially extensive under the free boundary condition,

which allowed free grain translations relative to each other. Under this condition, the GB motion had the character of a nearly random walk, during which some GBs could wander far away from their initial position, especially at high temperatures.

The spontaneous GB motion was often found to be coupled to grain translations. When spontaneous GB motion was coupled, it always occurred at temperatures where stress-driven motion was also coupled. Fig. 12 illustrates the strong coupling of the Σ17(5 3 0) GB at 800 K. This plot shows that there is a close correlation between the grain translations (which occur in opposite directions by equal amounts) and the normal GB motion. Furthermore, by plotting the relative grain translation against the GB displacement, the coupling factor β was estimated and was found to be in good agreement with results of stress-induced simulations. Note that the random walk velocity at this temperature can be about 1 m/s, which is compatible with the imposed velocities in our stress-driven simulations.

In one of the runs performed at 1200 K, the Σ17(5 3 0) boundary was observed to reach one of the free surfaces and disappear on it, turning the simulation block into a single crystal. Interestingly, when this GB was about 1 nm away from the surface, the material confined between the GB and the surface quickly turned into metastable melt, which then crystallized with the lattice orientation of the remaining grain. Other GBs were less mobile and never approached a surface.

The fixed boundary condition strongly suppresses the spontaneous GB motion but does not eliminate it completely. In this case, the grains can only translate at the expense of elastic deformation, which completely changes the character of the GB motion. Instead of a random walk, the GB now moves up and down around its average position with a correlation time and amplitude that depend on the particular GB misorientation, temperature and the system size in the normal direction.

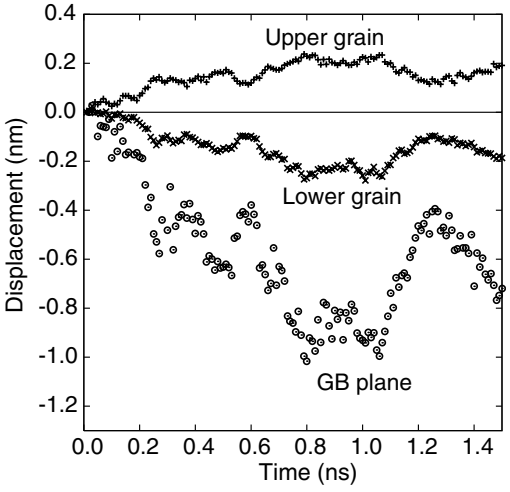

Fig. 12. Coupling during spontaneous motion of the Σ17(5 3 0) GB at 800 K. Simulations were performed with the free boundary condition.

7. Atomic mechanisms of coupled boundary migration

In the previous sections we saw that there are two modes of coupled GB motion differing in sign of β, that there can be a switch between them as the tilt angle is varied, and that there can be dual behavior in which the mode changes at a given θ. In this section we examine the atomic mechanisms of coupled GB motion and then relate the dual behavior to their change. Before explaining them, note that the perfect FCC lattice viewed along [0 0 1] can be thought of as containing many types of structural units. Two six-member units are relevant to this discussion, which we label as B and C as indicated in Fig. 13. The black and white circles represent atomic rows with different depths of atomic positions. The six-member kite-shaped units forming the GB structure are referred to as units A (see examples in Fig. 4). Note that black and white circles alternate in units A and B while unit C has three adjacent circles with the same color.

The atomic mechanisms of coupled GB motion were determined by examining multiple snapshots stored during the MD simulations along with relevant parts of atomic trajectories. Two different types of mechanisms were found, corresponding to GB motion in the ⟨1 0 0⟩ and ⟨1 1 0⟩ modes.

A typical ⟨1 1 0⟩ mode mechanism is illustrated in Fig. 14 using the zigzag Σ17(5 3 0) GB as an example. Note a structural unit B adjacent to every GB unit A (Fig. 14(a)). The two units can be transformed by relatively small in-plane atomic displacements, so that B becomes a kite and A becomes a B unit in the upper grain. If this transformation happens in every other GB unit, the boundary makes one step down while the upper grain translates to the right in order to accommodate the unit deformations (Fig. 14(c)). The transition state of this process is a mirror-symmetrical structure shown in Fig. 14(b). Similar mechanisms operate in all other GBs moving in the ⟨1 1 0⟩ mode up to some differences in relative positions of the A and B units. In GBs with a planar stacking of the A units, the A–B transformations occurs in all such units simultaneously (see examples in Fig. 15). In low-angle GBs with θ approaching 90°, this mechanism represents collective glide of an array of $-1/2[1\,1\,0]$ lattice dislocations along $(\bar{1}\,1\,0)$ planes. The A–B transformations within the dislocation cores represent elementary steps of the dislocation glide.

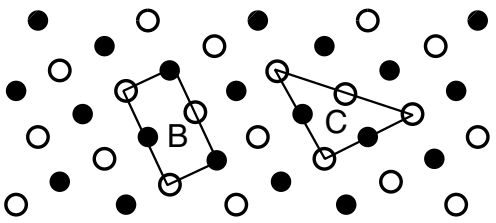

Fig. 13. Perfect fcc lattice viewed along the [0 0 1] direction can be thought of as composed of structural units B or C.

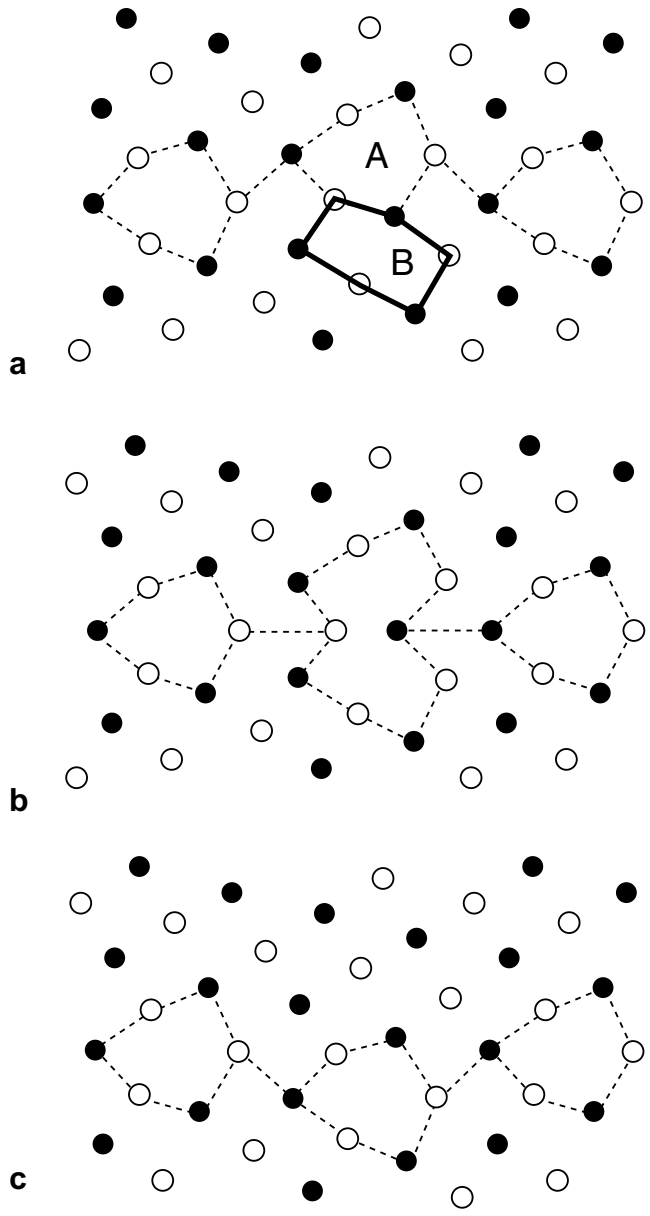

Fig. 14. Atomic mechanism of coupled motion of the Σ17(530) GB. (a) Initial state; (b) transition state; (c) final state. B is the lattice structural unit converting to the GB unit A.

A typical ⟨100⟩ mechanism of GB migration is illustrated in Fig. 16 for the Σ37(610) GB. Consider the structural unit C interlocked with the kite-shaped GB unit A. Unit C can be transformed to A by in-plane and out-of-plane atomic displacements bringing atomic row 1 to the same depth as row 2. The GB moves by translating this row by $\pm a/2$ along the tilt axis with simultaneous small deformations of both units. Since the row translations by $1/2[001]$ and $1/2[00\bar{1}]$ are symmetrically equivalent, this mechanism cannot operate at 0 K. Finite temperatures can break the symmetry and activate this mechanism. Whether the directions of row translations in neighboring kite units correlate with each other depends on their separation and temperature, but this aspect was not studied in this work.

For low-angle GBs with small θ, this mechanism is equivalent to collective glide of the [100] dislocations along (010) planes. Note that the dislocation core moves along the slip direction by a vector $1/2[100]$ at a time. This motion can be understood if we consider a [100] dislocation as narrowly dissociated in two perfect lattice dislocations by the reaction

$$[100] \leftrightarrows 1/2[101] + 1/2[10\bar{1}] \quad (6)$$

and moving by correlated displacements of both product dislocations. Since both product dislocations have a screw component parallel to the tilt axis, their motion involves a shuffling of atomic rows parallel to that direction. Which dislocation is leading and which is trailing are two symmetrically equivalent possibilities. This choice dictates the sense of the direction of the row translation in unit C (up-down or down-up).

The common idea of all these mechanisms is that structural units experience distortions as they are overrun by a moving GB. These distortions have three components: local atomic displacements, rotation of the atomic groups forming the units and translation of their centers of mass. The structural unit first turns into a GB unit A, and as the GB moves on, the distortions continue until the unit finally transforms back into a lattice unit left behind the moving GB. This new structural unit has a different location and orientation with respect to the initial one. In addition, there is a clockwise or counterclockwise (depending on the sense of the stress) cyclic permutation of atoms within the unit. Importantly, this mechanism does not require diffusion. At 0 K it only requires a critical stress to be reached. Thermal activation at finite temperatures permits operation of this mechanism at lower stresses. For low-angle GBs, the atomic shuffling only occurs when a lattice unit is overrun by a moving dislocation core. The units between the dislocations only experience small elastic strains and rotations.

Inspection of all GB structures reveals that lattice units B and C exist next to any GB unit A. Thus, purely geometrically the unit transformations can proceed by either of the two mechanisms. The actually operating mechanism is the one with the smaller critical stress. However, the fact that any GB is structurally "prepared" to move in either of the two coupling modes is essential for understanding the dual behavior of GBs and the multivalued character of the coupling factor.

The origin of the dual behavior is in the fact that the activation of the ⟨100⟩ mode requires breaking the mirror symmetry, which is blocking the row translations involved in the GB migration. At low temperatures breaking the symmetry takes significant time. Examination of MD snapshots also reveals that the switch to the ⟨100⟩ mode does not occur until the GB structure develops steps, ledges and other defects, which presumably assist in breaking the symmetry.

The atomic mechanisms just described explain the coupled GB motion by transformations of structural units.

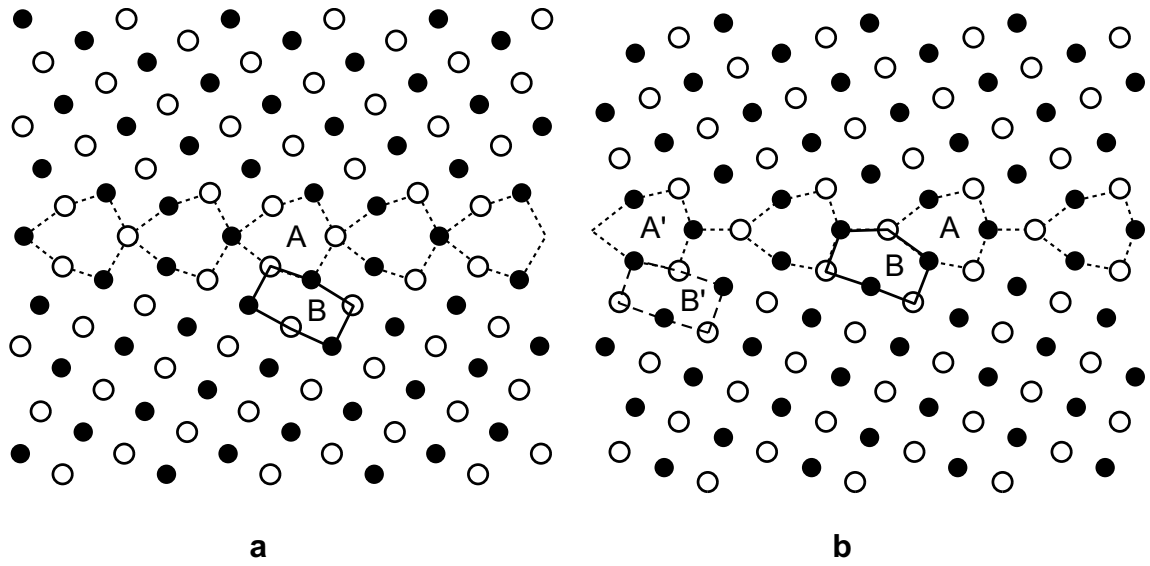

Fig. 15. Atomic mechanisms of coupled motion of the (a) Σ5(210) and (b) Σ5(310) GBs. In both cases B is the lattice structural unit converting to the GB unit A. An alternative mechanism for the Σ5(310) GB could involve the units A′ and B′, but this mechanism is never observed.

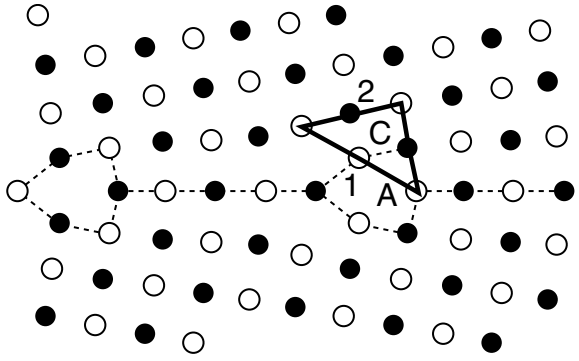

Fig. 16. Atomic mechanism of coupled motion of the Σ37(610) GB. C is the lattice structural unit converting to the GB unit A. 1 and 2 are atomic rows normal to the viewer discussed in the text.

In reality, such transformations are unlikely to happen simultaneously in all units over a large GB area. MD simulations reveal that GBs typically move by a nucleation and growth mechanism initiated by the formation of a relatively small area over which the GB has advanced ("embryo"). The "embryo" is separated from the rest of the boundary by a one-dimensional defect, which can be identified as a GB disconnection [42–44]. Sidewise propagation of the disconnection loop eventually results in a normal displacement of the entire boundary by one elementary step H, accompanied by a tangential grain translation by S. Crystallographic characteristics of the disconnections will be discussed later (Section 9.5) and their effect on GB dynamics will be the subject of a separate publication.

The formation of a critical "embryo" is a thermally activated process, which can either occur spontaneously or be driven by an applied shear stress. At a critical level of the stress, the nucleation activation barrier is eliminated and the boundary migration becomes athermal. It should be Imentioned that the disconnection loops were only observed in MD simulations with large lateral dimensions of the simulation block. In small blocks, the boundary displacements took place uniformly over the entire GB area.

8. Transition between coupling and sliding

So far we have only examined conditions under which the GB response to applied shear was perfect coupled motion. We will now consider situations when the response changes, partially or completely, from coupling to sliding with increasing temperature.

MD simulations of stress-driven GB motion were performed at temperatures up to ~30 K below the bulk melting point T_m ($T_m = 1327$ K) with this embedded-atom potential [41]; the experimental value for copper is 1358 K. Above about 800 K the coupled GB motion begins to be interrupted by occasional sliding events as illustrated in Fig. 17. Such events are identified as sliding because they are accompanied by relative grain translations and a drop of stress without normal GB displacement. Between the sliding events, the GB continues to move in a coupled mode with a characteristic geometric value of β. This suggests that the GB sliding occurs by a mechanism that preserves the boundary structure. As the temperature increases further, the relative frequency of the sliding events increases and thus the average normal velocity v_n decreases. In high-angle GBs, at high enough temperatures the coupled motion ceases to be observed and sliding becomes the dominant mode of the GB response, although the GB continues to execute random movements over small distances. Under such conditions we assign v_n a zero value.

Fig. 18 shows the temperature dependence of the velocity ratio $v_n/v_\parallel$ calculated for different GBs with the same shear rate $v_\parallel = 1$ m/s. The tilt angle increases monotonically from

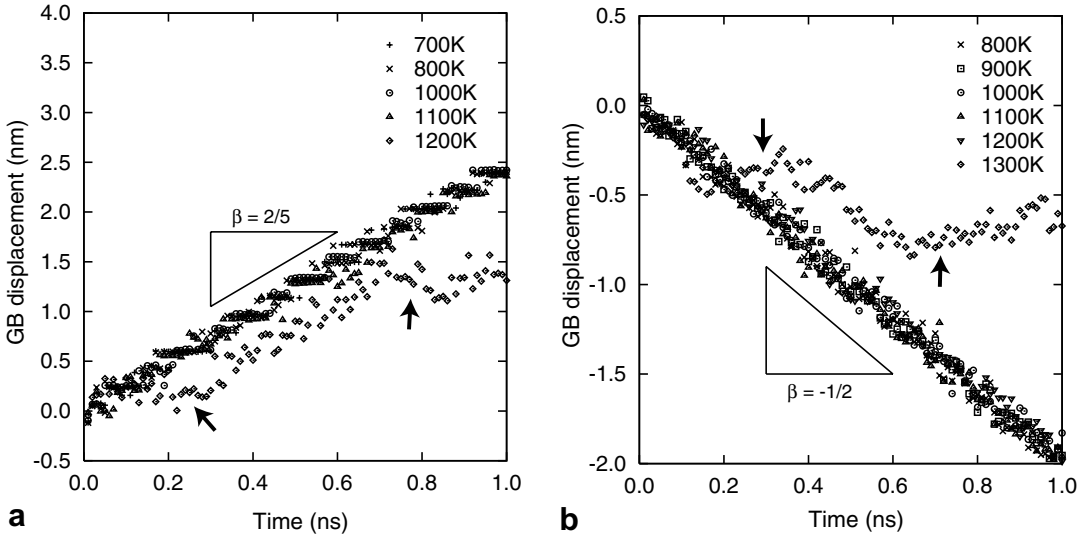

Fig. 17. Displacements of the (a) Σ13(510) and (b) Σ17(530) GBs as functions of time at selected temperatures. The imposed shear rate is 1 m/s. The arrows indicate nearly horizontal regions corresponding to individual sliding events.

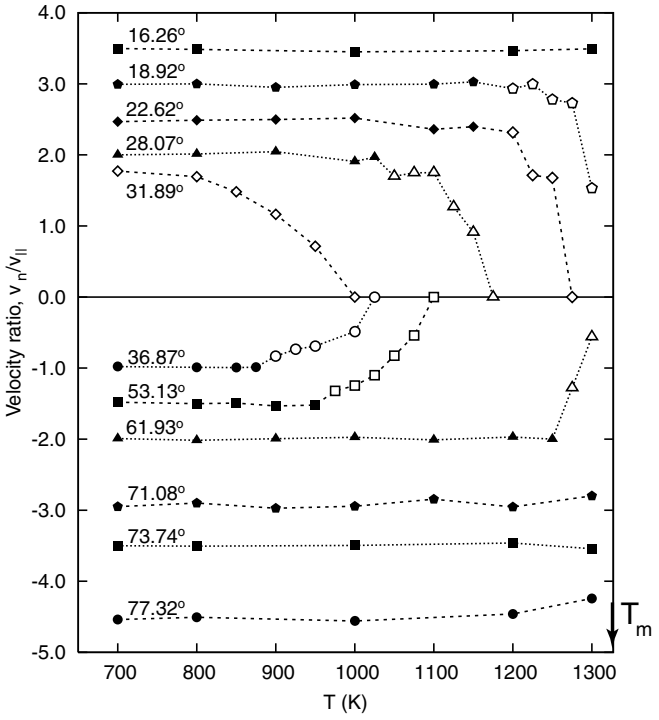

Fig. 18. Temperature dependence of the velocity ratio $v_n/v_\parallel$ obtained by MD simulations with the shear rate $v_\parallel = 1$ m/s. Open symbols indicate temperatures at which GB sliding events were observed. T_m is the bulk melting temperature.

the upper curves to the lower ones. At relatively low temperatures $v_n/v_\parallel$ remains practically constant and matches the geometric value of $1/\beta$, which confirms that the coupling is perfect. For high-angle GBs there is a temperature, which we refer to as the crossover temperature, at which $|v_n/v_\parallel|$ begins to decrease due to random switches between coupling and sliding. The scatter of $v_n/v_\parallel$ values in the crossover regime is due to the limited statistics collected under conditions when only a few sliding events could happen during an MD run. Above the crossover temperature range, sliding dominates over coupling. These data can be mapped onto the diagram of mechanical responses, Fig. 8, creating a domain of sliding separated from the coupling domains by relatively narrow crossover regions.

To check whether the crossover from coupling to sliding is sensitive to $v_\parallel$, the calculations for the Σ5(210) GB were repeated with a shear rate of 0.5 m/s. The temperature dependence of $v_n/v_\parallel$ obtained, and thus the crossover temperature, were found to be nearly the same as for $v_\parallel = 1$ m/s. This observation only indicates that the results shown in Fig. 18 are not extremely sensitive to $v_\parallel$; we cannot, however, exclude their shear-rate dependence under much greater variations in $v_\parallel$.

The observation of the crossover regime indicates that coupling and sliding can coexist in the same GB, which validates our postulated Eq. (1). Furthermore, because $\beta(\theta)$ is known from both theory and low-temperature simulations, we are in a position to evaluate the sliding component v_s of the grain translation velocity by rearranging Eq. (1):

$$v_s = v_\parallel - \beta(\theta) v_n. \tag{7}$$

Since $v_\parallel$ is imposed and v_n is measured by the simulations, the right-hand side of this equation is known and we can deduce v_s. We can also introduce the quantity

$$\zeta \equiv \frac{v_s}{v_\parallel} = 1 - \frac{\beta v_n}{v_\parallel}, \tag{8}$$

which characterizes the fraction of $v_\parallel$ associated with sliding events. (Note that β has the same sign as the ratio $v_n/v_\parallel$, so that $\beta v_n/v_\parallel$ is always positive.)

Fig. 19 displays the temperature dependencies of ζ for various GBs. As expected, high-angle GBs show a rapid increase in ζ in the crossover temperature range and eventually reach the condition $\zeta \approx 1$ (pure sliding). For low-angle

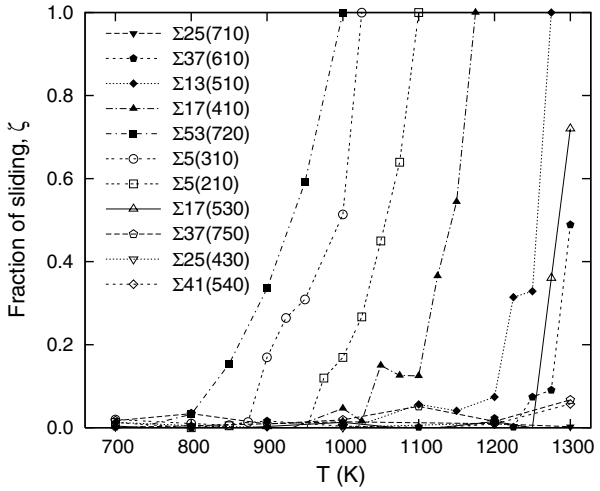

Fig. 19. The fraction of sliding as a function of temperature for selected GBs. The GBs are listed in increasing tilt angle.

GBs, ζ remains practically zero until the melting point. Using the criterion $\zeta = 0.5$ as a definition we can quantify the crossover temperature. If this condition is never satisfied, we identify the crossover temperature with T_m for this discussion. Fig. 20 shows that this crossover temperature reaches a minimum of about $0.7T_m$ in the high-angle region, where β changes sign. Although these estimates of the crossover temperatures relative to T_m are obtained for Cu, we expect them to be valid for other metals as well.

We expect that the critical stresses for coupling and sliding for the same θ are different, and that both are temperature-dependent. The coupling to sliding transition can be explained by a crossover of the respective critical stresses. Note that the temperature range of the crossover regime is wider when it occurs a lower temperatures. This is contrary to what one would expect for Arrhenius behavior of two competing reactions with different but temperature-independent barriers. In our case, however, the barriers and the critical stresses do vary with temperature.

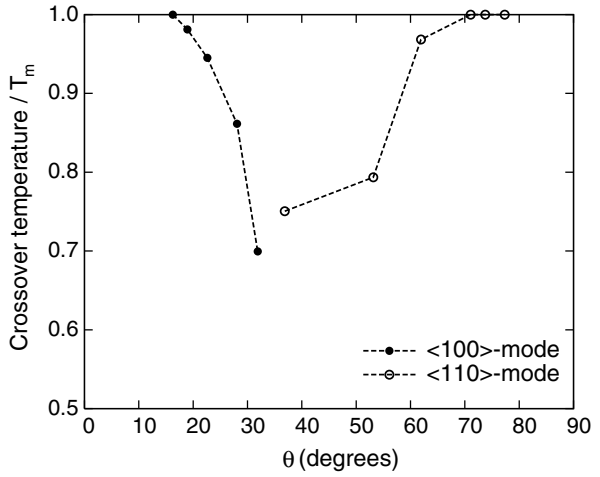

Fig. 20. The coupling-to-sliding crossover temperature, normalized by the melting temperature T_m, as a function of the tilt angle θ. The coupling modes of the GBs are indicated.

To put these observations in a different perspective, choose a temperature, e.g., $0.85T_m$ (~1100 K for Cu), for which sliding dominates at high tilt angles. Suppose we vary the tilt angle of a planar boundary gradually from 0 to 90° under a fixed $v_\parallel$. The diagram of mechanical responses, Fig. 8, predicts that the boundary will initially be moving with perfect coupling in the small-angle $\langle 1\,0\,0\rangle$ mode ($\beta \approx \theta > 0$). As θ increases, individual sliding events will begin to happen, which will reduce the average v_n. At some point the GB response will switch completely from coupling to sliding and the GB will stop moving, although small random displacements may still be observed. At larger angles, coupling events will begin to be seen, but now they will be driving the GB in the opposite direction ($\langle 1\,1\,0\rangle$ mode, $\beta < 0$). Finally, with θ approaching 90° we will arrive at a low-angle GB moving with a perfect coupling factor $\beta \approx \theta - \pi/2 < 0$.

A similar situation may have been realized during the simulations of the shrinkage and rotation of an enclosed cylindrical grain when the temperature was about 2/3 of the melting point of the Lennard-Jones solid [31]. This temperature is large enough to give rise to sliding in high-angle GBs, which may explain the observed gradual reduction in the rotation velocity at large tilt angles relative to its ideal value βv_n.

9. Geometric models of coupling

9.1. General considerations

The goal of this section is to relate the coupling factor β and the increments H and S of GB motion to crystallographic characteristics of symmetrical tilt GBs. We will also show how the multiplicity of possible geometric descriptions of the same GB, arising from point symmetry of the crystal lattice, leads to the multivalued character of β, H and S.

As a GB moves, it produces a rotation of the lattice of the receding grain into the orientation of the growing grain. The essence of the coupling effect is that this lattice reorientation is accompanied by a specific shape deformation of the material. If we label atoms residing within a relatively large ("macroscopic") material region in front of the moving GB, the shape of this region will be altered by the passage of the GB. In the case of ideal coupling, the shape change of any such region can be described by a unique deformation tensor, **D**, which depends on crystallographic characteristics of the GB. For a planar tilt GB, the shape deformation **D** is a simple shear parallel to the GB characterized by a coupling factor β, with the GB plane being the invariant plane of the shear.[6] Any other type of deformation would produce a long-range elastic strain field in the grains.

[6] For a boundary with a twist component, **D** can also include a rotation around the boundary normal.

This situation is formally similar to diffusionless transformations [45,46], except that the lattices of the parent and product "phases" are identical and only differ in their crystallographic orientations. Furthermore, for the [001] tilt GBs studied here, there is no homogeneous strain carrying one orientation of the fcc lattice to another with a common [001] axis. Therefore, inhomogeneous plastic deformation, e.g., by the passage of dislocations, is the only type of lattice-invariant deformation that can produce the transformation. It follows that **D** must be an appropriate combination of lattice rotation and lattice-invariant plastic deformation. In the case of low-angle GBs, the latter component of the deformation is implemented by slip of discrete lattice dislocations forming the GB structure. This dislocation model of coupling will be discussed in Section 9.2. In high-angle GBs, the notion of discrete lattice dislocations loses its significance. The Burgers vector content is then prescribed by the Frank–Bilby equation [1,47–49], which has multiple solutions. Borrowing from the theory of martensitic transformations [45,49,50], we will show in Section 9.3 how the shape deformation, and thus the coupling factor, can be calculated as functions of the lattice misorientation across the boundary. Finally, in Sections 9.4 and 9.5 we demonstrate that β, H and S of CSL boundaries can be associated with particular vectors of the displacement shift complete lattice for both low and high-angle GBs.

9.2. Discrete dislocation model of coupling

One way to describe the coupling effect is to explicitly consider the dislocation structure of the GB and postulate that it is the glide of the GB dislocations that produces the shear deformation accompanying the GB motion. For low-angle, symmetrical-tilt GBs, this dislocation model was first proposed by Read and Shockley [32] and later discussed in more detail by Read [51]. By analyzing glissile motion of such boundaries in a simple cubic lattice under an applied shear stress, Read and Shockley derived the expression $2\tan(\theta/2) \approx \theta$ for the coupling factor. Building upon the Read and Shockley model, we will derive expressions for β, H and S for [001] symmetrical tilt GBs in fcc crystals and will compare the results with our simulations.

Consider a GB whose tilt angle θ is small enough to resolve discrete GB dislocations (see e.g., Fig. 4(a)). As was established by the simulations, the dislocations in such GBs have the Burgers vector $\mathbf{b} = [100]$ and glide along (010) slip planes. While the magnitude of this Burgers vector is uniquely defined, its direction is not unique and depends on the arbitrary choice of the orientation of the reference lattice, used in the Burgers circuit construction, relative to the bicrystal. Frank [47] proposed to refer the Burgers vector to the median lattice whose $\theta/2$ and $-\theta/2$ rotations produce the upper and lower grains, respectively. The Burgers vector is then normal to the GB plane. For our purposes, however, assuming that the GB moves up, it is more appropriate to choose the upper grain as the reference lattice, because it is the dislocation glide through that grain that produces the shear deformation. With this choice of the reference lattice, the Burgers vector is parallel to [100] of the upper grain and therefore forms the angle $\theta/2$ with the GB normal in the counterclockwise direction. The spacing L between neighboring dislocations must satisfy the Frank equation [47]

$$b/L = 2\sin(\theta/2), \tag{9}$$

where in the present case $b = a$. This equation expresses the fact that the dislocations are intrinsic, i.e., geometrically necessary for accommodating the tilt θ without producing long-range elastic stresses in the grains.

Consider a block of material, OABC, whose horizontal faces are initially parallel to the GB plane and whose sides are parallel to the dislocation slip planes (Fig. 21(a)). Let the GB segment OA comprised by the block have a unit length and therefore contain $\rho = 1/L$ dislocations. The shape deformation of the block as it is traversed by the GB can be thought of as occurring in two steps. First, the block is sheared by the passage of the GB dislocations

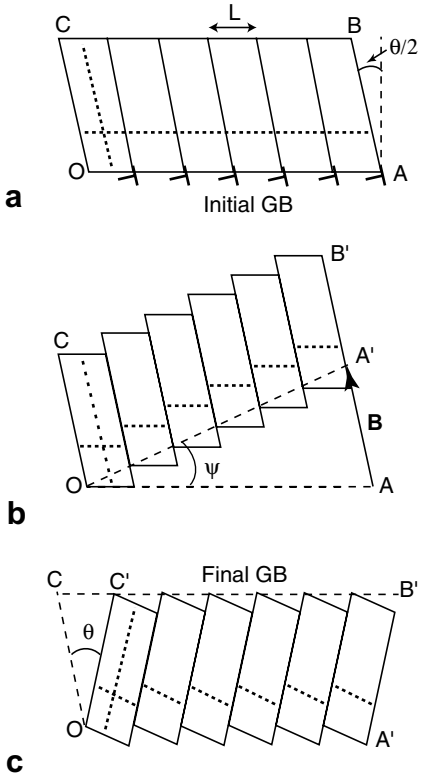

Fig. 21. Dislocation mechanism of coupled motion of tilt GBs. (a) A block of material OABC with sides parallel to the dislocation slip planes. (b) The passage of the GB upwards produces a shear deformation of the block to a new shape OA′B′C. To close the void OAA′, the block rotates by the angle ψ. (c) Final GB position. Due to the Frank equation, $OA = OA'$ and $\psi = \theta$. The final macroscopic shape of the block is a mirror reflection of the initial one. The dotted lines show atomic planes whose atoms are labeled to follow their motion. Notice that the initially horizontal atomic plane remains on average horizontal but breaks into tilted segments.

without changing its lattice orientation. Assuming that point O is fixed, the block experiences the plastic deformation shown in Fig. 21(b). Side AB undergoes a parallel displacement by the total Burgers vector of the dislocations, $\mathbf{B} = \rho\mathbf{b}$, while the segment OA rotates by an angle ψ to a new position OA′.

At the second step, the block rotates clockwise by the tilt angle θ to align the lattice within the block with the lattice of the lower grain. This rotation aligns [1 0 0] directions of both grains parallel to each other. To maintain the contiguity of the material, this rotation must close the void OAA′ existing at the GB. This void does close perfectly since, by Eq. (9), the length of the side OA is conserved and $\psi = \theta$. If the sides OA and OA′ were different, a tensile strain would be required to close the void and the GB motion would produce a long-range elastic strain field. As mentioned above, the Frank equation (9) guarantees that such fields do not arise.

In reality, the shear and rotation steps occur simultaneously. The resulting shape change of the block represents a simple shear parallel to the GB plane (Fig. 21(c)). It follows that the angles formed by the sides OC and AB with the GB normal before and after the deformation are $\theta/2$ and $-\theta/2$, respectively. From the symmetry of the triangle OCC′ we immediately obtain the coupling factor

$$\beta_{\langle 1\,0\,0\rangle} = 2\tan(\theta/2). \tag{10}$$

This factor is positive by our sign convention and represents the ⟨1 0 0⟩ mode of coupling.

The [1 0 0] dislocations advance along the slip direction by increments of $a/2$ (Fig. 16). Therefore, each step of the GB motion is accompanied by a normal displacement

$$H_{\langle 1\,0\,0\rangle} = (a/2)\cos(\theta/2) \tag{11}$$

and a tangential translation of the upper grain to the right by

$$S_{\langle 1\,0\,0\rangle} = a\sin(\theta/2). \tag{12}$$

These relations are readily derived from the triangle OCC′ assuming $\mathrm{OC} = \mathrm{OC}' = a/2$.

As indicated in Fig. 21, the shear deformation produced by the dislocations is inhomogeneous. Atomic layers parallel to the dislocation slip planes rotate by the angle θ but otherwise remain undistorted. By contrast, layers parallel to the GB plane break into segments confined between neighboring slip planes and each segment rotates by the angle θ individually. In fact, all atomic layers that are not parallel to the slip planes break into segments. This segmentation is caused by the inhomogeneous atomic movements (“shuffling”) at the slip planes during the dislocation glide. The segmentation of atomic planes was verified in the atomistic simulations by labeling atoms residing in particular planes and plotting their new positions after they were swept by a moving GB.

Despite the segmentation, any layer of labeled atoms which is initially parallel to the GB plane remains on average parallel to it after the deformation. This is consistent with the notion that the shape deformation is a macroscopic property defined by averaging over atomic-level details. It is only on this macroscopic scale that the deformation produced by the GB represents pure shear and that the GB plane is the invariant plane of this shear.

This model is readily extended to GBs with θ approaching 90°. In this case, the GB dislocations have the Burgers vector $\mathbf{b} = -1/2[1\,1\,0]$ (e.g., Fig. 4(d)) and glide along $(\bar{1}\,1\,0)$ planes. A schematic illustrating the shear deformation produced by these dislocations is not shown here but can be obtained by a 180° rotation of Fig. 21 around the axis normal to the viewer, with a replacement of θ by $\varphi = 90° - \theta$. The Frank equation now becomes

$$b/L = 2\sin(\varphi/2), \tag{13}$$

where $b = a/\sqrt{2}$. As the GB moves down, the block OABC experiences a shear deformation parallel to the GB plane, accompanied by a translation of the lower grain to the left. In this process, the $[1\,\bar{1}\,0]$ direction of the lower grain rotates clockwise by the angle φ and becomes parallel to the [1 1 0] direction of the upper grain. Since the two directions are equivalent by cubic symmetry, the lattice remains continuous across the GB plane.

Assuming that the dislocations move by increments of **b** and repeating the preceding calculations, we obtain the increments of normal GB motion and grain translation

$$H_{\langle 1\,1\,0\rangle} = -(a/\sqrt{2})\cos(\varphi/2), \tag{14}$$

$$S_{\langle 1\,1\,0\rangle} = a\sqrt{2}\sin(\varphi/2). \tag{15}$$

Their ratio $\beta = S/H$ gives the expression for the coupling factor,

$$\beta_{\langle 1\,1\,0\rangle} = -2\tan(\varphi/2) \tag{16}$$

corresponding to the ⟨1 1 0⟩ mode of coupling. Note that $\beta < 0$.

This model has been verified by the MD simulations (Section 4). The coupling factors obtained perfectly follow Eq. (10) when θ is small and Eq. (16) when it approaches 90° (Fig. 7). More importantly, both equations continue to work perfectly well beyond the low-angle misorientations, suggesting that these equations have a more general meaning. This meaning will be discussed below.

9.3. Extended model of coupling

The discrete dislocation model discussed in the previous section essentially rests on the Frank equation, which relates the intrinsic Burgers vector density to the lattice misorientation across a low-angle GB. The Frank equation remains valid for high-angle GBs in a generalized form proposed by Bilby [48,49] in the context of his continuously dislocated crystal theory. In that theory, Eqs. (9) and (13) represent definitions of the intrinsic dislocation content which is formally assigned to a GB in order to accommodate the misorientation between the grains without producing long-range stresses. For a general GB, this formal dislocation content is characterized by a “surface dislocation density tensor”

and the entire GB is treated as one entity called a "surface dislocation" [48,49].

For a pure tilt GB, the surface dislocation density tensor can be replaced by a vector quantity **B**, which represents the total Burgers vector of all formal dislocations crossing a unit vector $\hat{\mathbf{p}}$ which lies in the GB plane and is normal to the tilt axis. If $\mathbf{R}_u$ and $\mathbf{R}_l$ are matrices of rotation of the upper and lower grains relative to a chosen reference lattice, the Frank–Bilby equation defining **B** reads[7]

$$\mathbf{B} = (\mathbf{R}_l^{-1} - \mathbf{R}_u^{-1})\hat{\mathbf{p}}. \tag{17}$$

A major problem associated with applications of this equation is the non-uniqueness of the dislocation content assigned to a GB. Indeed, point symmetry operations applied to the lattice of either grain can alter the rotations $\mathbf{R}_l$ or $\mathbf{R}_u$, and thus **B**, without changing the actual GB structure or energy.

As before, if the GB moves upwards, we choose the upper grain as the reference lattice. The lower grain is then obtained by a rotation $\mathbf{R} = \mathbf{R}_u\mathbf{R}_l\mathbf{R}_u^{-1}$ of the upper grain and Eq. (17) takes the form

$$\mathbf{B} = (\mathbf{R}^{-1} - \mathbf{I})\hat{\mathbf{p}}, \tag{18}$$

where **I** is the identity matrix. Applying the rotation **R** to both sides of this equation, we obtain a useful relation

$$\mathbf{RB} = \hat{\mathbf{p}} - \mathbf{R}\hat{\mathbf{p}}. \tag{19}$$

Represent **B** as $B\hat{\mathbf{g}}$, where $\hat{\mathbf{g}}$ is a unit vector parallel to **B**. We postulate that the "surface dislocation" is capable of gliding along the plane containing **B** and the tilt axis (Fig. 22). Let $\hat{\mathbf{m}}$ be the unit normal to this plane, so that $\hat{\mathbf{m}} \cdot \hat{\mathbf{g}} = \mathbf{0}$. Following Bullough and Bilby [50], we assume that the material swept by the "surface dislocation" undergoes a shape change $\mathbf{D} = \mathbf{RS}$ consisting of two components: (i) plastic deformation **S** performed without altering the lattice orientation, and (ii) lattice rotation by **R**. (A third component considered in [50] is a homogeneous lattice strain, which is absent in our case.) The role of the rotation is to align the lattice traversed by the GB parallel to the lattice of the lower grain. The role of the plastic deformation is to accommodate the shape change of the material and eliminate any long-range stresses.

To calculate **S**, consider a macroscopic vector **r** scribed in the upper grain and crossing the boundary at point O. Resolving it along $\hat{\mathbf{g}}$ and $\hat{\mathbf{p}}$ we have $\mathbf{r} = x\hat{\mathbf{g}} + y\hat{\mathbf{p}}$, where $x = (\mathbf{r} \cdot \hat{\mathbf{n}})/(\hat{\mathbf{g}} \cdot \hat{\mathbf{n}})$ and $y = (\mathbf{r} \cdot \hat{\mathbf{m}})/(\hat{\mathbf{g}} \cdot \hat{\mathbf{n}})$.[8] We postulate that under the transformation **S** the tip of **r** experiences a displacement **u** equal to the net Burgers vector, $y\mathbf{B}$, of all dislocations crossed by the parallel component $y\hat{\mathbf{p}}$. Thus,

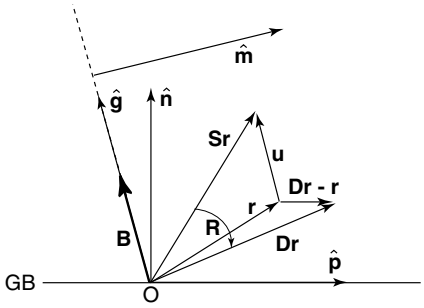

Fig. 22. The shape deformation **D** produced by a moving GB as a combination of shear **S** and rotation **R**, showing that $\mathbf{Dr} - \mathbf{r}$ is parallel to the GB. **r** is any macroscopic vector scribed in the upper grain.

$$\mathbf{u} = y\mathbf{B} = \beta(\mathbf{r} \cdot \hat{\mathbf{m}})\hat{\mathbf{g}}, \tag{20}$$

where we introduced

$$\beta \equiv \frac{B}{\hat{\mathbf{g}} \cdot \hat{\mathbf{n}}}. \tag{21}$$

Eq. (20) defines **S** through the relation $\mathbf{Sr} = \mathbf{r} + \mathbf{u} = (x + yB)\hat{\mathbf{g}} + y\hat{\mathbf{p}}$. It shows that **S** is a simple shear by β in the direction $\hat{\mathbf{g}}$ parallel to the slip plane $\hat{\mathbf{m}}$. Note that for any **r** lying in the plane $\hat{\mathbf{m}}$, Eq. (20) gives $\mathbf{u} = 0$, showing that $\hat{\mathbf{m}}$ is an invariant plane of this shear.

The total shape deformation **D** is now obtained by applying the rotation **R** to the deformed vector **Sr**

$$\mathbf{Dr} = \mathbf{RSr} = (x + yB)\mathbf{R}\hat{\mathbf{g}} + y\mathbf{R}\hat{\mathbf{p}}, \tag{22}$$

which after some manipulation using Eq. (19) becomes

$$\mathbf{Dr} = \mathbf{r} + (\mathbf{R}\hat{\mathbf{g}} - \hat{\mathbf{g}})\frac{\mathbf{r} \cdot \hat{\mathbf{n}}}{\hat{\mathbf{g}} \cdot \hat{\mathbf{n}}}. \tag{23}$$

It can be shown (see Appendix) that $\mathbf{R}\hat{\mathbf{g}} - \hat{\mathbf{g}} = B\hat{\mathbf{p}}$, which allows us to rewrite Eq. (23) as

$$\mathbf{Dr} = \mathbf{r} + \beta(\mathbf{r} \cdot \hat{\mathbf{n}})\hat{\mathbf{p}} \tag{24}$$

with β given by Eq. (21). This relation shows that the shape deformation produced by the moving boundary is indeed simple shear by β parallel to the GB plane and normal to the tilt axis. The GB plane is an invariant plane of the shear, since for any **r** lying in the GB plane we have $\mathbf{r} \cdot \hat{\mathbf{n}} = 0$ and Eq. (24) gives $\mathbf{Dr} = \mathbf{r}$.

Eq. (21) predicts coupling factors for both low- and high-angle misorientations. As mentioned above, β and **B** are not unique due to the point symmetry of the crystal. For example, we can choose **R** as a clockwise rotation by the smallest possible angle θ. Then the Frank–Bilby equation (18) dictates that **B** has the magnitude $B = 2\sin(\theta/2)$ and forms the angle $\theta/2$ counterclockwise with respect to $\hat{\mathbf{n}}$. This makes **B** parallel to the [1 0 0] direction of the upper grain, so that the "surface dislocation" glides along (0 1 0) planes. We then have $\hat{\mathbf{g}} \cdot \hat{\mathbf{n}} = \cos(\theta/2)$ and Eq. (21) gives $\beta = 2\tan(\theta/2)$, an expression which was previously derived for the $\langle 1\,0\,0 \rangle$ mode of coupling within the discrete dislocation model.

On the other hand, this rotation **R** can be combined with a counterclockwise 90° rotation of the lattice of the lower

[7] In Bilby's original theory [48,49] the matrices $\mathbf{R}_u$ and $\mathbf{R}_l$ represent arbitrary lattice transformations which may include not only rotations but also homogeneous lattice strains. This general form of the theory applies to both GBs and interphase interfaces. For the present discussion we limit the transformation matrices to lattice rotations around the tilt axis.

[8] The component of **r** parallel to the tilt axis is invariant under all transformations and can be safely disregarded.

grain around [0 0 1], which is a point-symmetry operation that cannot affect the GB structure. With this new choice of **R**, **B** becomes parallel to the $[\bar{1}\,\bar{1}\,0]$ direction of the upper grain and has the magnitude $B = 2\sin(\varphi/2)$, where $\varphi = 90° - \theta$. The "surface dislocation" now glides along $(\bar{1}\,1\,0)$ planes, which corresponds to the $\langle 1\,1\,0\rangle$ mode of coupling. Considering that $\hat{\mathbf{g}} \cdot \hat{\mathbf{n}} = -\cos(\varphi/2)$, Eq. (21) yields $\beta = -2\tan(\varphi/2)$, which is the familiar $\langle 1\,1\,0\rangle$ mode expression derived earlier within the discrete dislocation model. Thus, the shift of the rotation angle θ by 90° gives rise to a new mode of GB motion, in which the lattice of the receding grain rotates by the angle $\theta - 90°$ instead of θ. Formally, two more branches of $\beta(\theta)$ could be obtained by shifting θ by $-180°$ and $-270°$, but they are unlikely to be realized in experiments or simulations since they require larger lattice rotations than the previous two.

Thus, using the concept of a "surface dislocation" and the formal analogy with martensitic transformations, we have extended the discrete dislocation model of coupling to high-angle GBs. In the limiting cases of low-angle GBs arising at the ends of the misorientation range, we correctly recover the expressions for $\beta(\theta)$ obtained within the discrete dislocation model. The extended model therefore predicts that those expressions continue to be valid across the entire misorientation range, which was indeed verified by atomistic simulations (Fig. 7). This analysis also demonstrates that the multivalued character of β originates from the invariance of the GB structure under point symmetry operations in the grains.

Another important feature of the extended model is that it does not require that the GB be symmetrical. The model predicts that the coupling factor only depends on the tilt angle but not on the GB plane inclination. We are in the process of testing this prediction by atomistic simulations. A low-angle asymmetrical tilt GB of the [0 0 1] family contains a mixed array of $\langle 1\,0\,0\rangle$ and $1/2\langle 1\,1\,0\rangle$ dislocations. It is not immediately clear how the dislocations having different Burgers vectors and gliding along intersecting slip planes can conspire to move together and maintain the same GB structure without locking each other. Besides dislocation glide, this motion may involve other processes such as cross-slip and dissociation–recombination reactions between the dislocations. Read and Shockley [32,51] suggested that glissile motion of asymmetrical GBs would be impossible, but no convincing proof of this conjecture was presented.

9.4. Increments of boundary motion

The dislocation model discussed in Section 9.2 also predicts the multiplicity of the increments, H and S, of the coupled GB motion. Fig. 11 displays the misorientation dependencies of H and S calculated from the dislocation model and compared with results of atomistic simulations. Two interesting features are revealed by this plot.

Firstly, excellent agreement is observed between predictions of the dislocation model and MD results for both coupling modes, not only for low-angle GBs but across the entire misorientation range. We again observe that the dislocation model proposed for low-angle GBs continues to work for high-angle misorientations, despite the fact that individual dislocations can no longer be resolved.

Secondly, while H and S obtained for flat GBs perfectly agree with Eqs. (14) and (15), the values for zigzag GBs are exactly half of those predictions and thus fall on a separate curve. This indicates that zigzag GBs actually move by increments of **b**/2 and not **b** as was assumed in deriving Eqs. (14) and (15). As a result, the $\langle 1\,1\,0\rangle$ branches of $H(\theta)$ and $S(\theta)$ split in two sub-branches corresponding to flat and zigzag GBs. The only exception is the $\Sigma 5(3\,1\,0)$ GB, which has a planar structure but still lies on the zigzag sub-branch. We emphasize that both sub-branches are characterized by the same coupling factor $\beta(\theta)$.

The origin of this difference between the flat and zigzag GBs can be understood from the atomic mechanisms of their motion. A zigzag GB structure can be considered as being split into two layers formed by the structural units, as illustrated in Fig. 14. Such boundaries always move in the $\langle 1\,1\,0\rangle$ mode by translating one layer of structural units at a time. Although the layer moves by the full Burgers vector **b**, the GB plane (which can be identified as a median plane between the two layers) only translates by **b**/2. By contrast, during the $\langle 1\,1\,0\rangle$ motion of flat GBs all structural units translate by **b** simultaneously (see example in Fig. 15(a)).

The $\Sigma 5(3\,1\,0)$ GB presents a special case. By analogy with other flat GBs one could expected it to move by A′–B′ unit transformations as indicated in Fig. 15(b). This would lead to H and S values consistent with Eqs. (14) and (15). However, the actual motion of this GB involves the lattice unit B situated one (3 1 0) layer closer to the GB plane, resulting in H and S which are twice as small.

It is interesting to note that all boundaries lying on the lower sub-branch (dash-dotted line in Fig. 11) belong to the class of centered GBs [37] with $h^2 + k^2 = 2\Sigma$ (both h and k are odd), whereas the higher sub-branch is populated by non-centered GBs ($h^2 + k^2 = \Sigma$). Because in any small vicinity of a centered misorientation there are non-centered ones and vise versa, the functions $H(\theta)$ and $S(\theta)$ corresponding to the $\langle 1\,1\,0\rangle$ mode of coupling are not only multivalued but also non-analytical.

9.5. Disconnections at grain boundaries

As discussed in Section 7, the motion of a planar GB under an applied shear stress is unlikely to happen uniformly over a large area. Rather, an area of a critical nucleus size should first undergo a normal displacement and expand by spreading sidewise in a manner similar to the nucleation and growth of a new "phase". The shear stress provides the driving force of this process and plays a role similar to the undercooling in a first-order phase transformation. The critical nucleation size is dictated by a balance between the elastic strain energy released due

to the local grain translation and the excess energy associated with the line defect surrounding the displaced GB region.

Due to the coupling effect, the lattice regions separated by this line defect are in different translational states parallel to the boundary plane. Hence, there is a dislocation content associated with this line defect, with a Burgers vector **S** lying parallel to the GB plane. For tilt GBs, the Burgers vector must be normal to the tilt axis. On the other hand, the defect separates GB regions that have identical atomic structures but lie in different (but parallel) planes. This makes this defect similar to a GB step. An interfacial defect possessing a combined step and dislocation character is classified as a disconnection [42] and is commonly observed at the growth front of massive transformations [42–44]. Thus, the step height of the disconnection is H and the magnitude of the Burgers vector is S which were introduced in Section 9.2.

For the particular cases of CSL GBs, the disconnection characteristics S and H can be associated with appropriate vectors of the displacement shift complete (DSC) lattice of the bicrystal. This was pointed out by King and Smith [52] who did not use the term disconnection but did show that step vectors associated with extrinsic GB dislocations must belong to the DSC.

As an example, Fig. 23 displays a [0 0 1] projection of the three-dimensional dichromatic pattern corresponding to the Σ5 misorientation of black and white fcc lattices, together with the CSL and DSC lattices that arise. A Σ5(2 1 0) GB lying in the plane ABC can be obtained by discarding all black atoms above this plane and all white atoms below it. Suppose all white atoms whose ordinate is positive and abscissa is the same as for point D or smaller

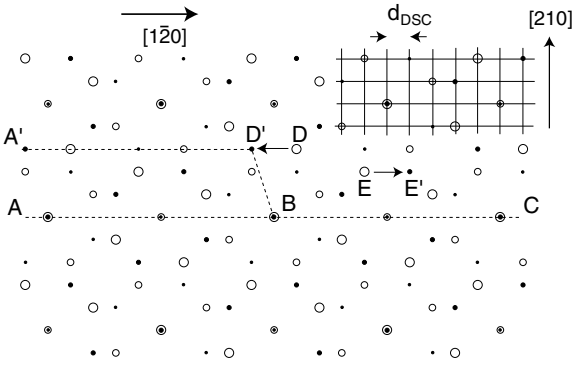

Fig. 23. Dichromatic pattern for the Σ5 misorientation of two (black and white) fcc lattices. The large and small symbols designate atomic positions in alternating (0 0 2) planes parallel to the page. The initial plane of a Σ5(2 1 0) GB is ABC, with white atoms occupying the upper grain and black atoms occupying the lower grain. After a translation of the left half of the white lattice by vector DD′ to the left, the GB plane develops a step BD′ and becomes A′D′BC. This step is associated with a Burgers vector DD′ and represents a disconnection. A propagation of the disconnection to the right constitutes a mechanism of GB motion in the ⟨1 1 0⟩ coupling mode. The ⟨1 0 0⟩ coupling mode could be implemented through the motion of another disconnection with the Burgers vector EE′. To avoid overloading the plot, the DSC grid is only outlined in the top right corner.

are shifted by the vector DD′, while all atoms on the right of D remain intact. Since vector DD′ belongs to the DSC lattice, this shift destroys the initial CSL on the left of point D but recreates it in a new position. Because point D′ now becomes a coincident site, the new CSL position can be considered as shifted relative to the initial one by vector BD′. As a result of this shift, the GB part AB moves to a new position A′D′ and the GB plane becomes A′D′BC with a step BD′. The height of this step equals $H = 3d_{DSC}$, where $d_{DSC} = a\sqrt{5}/10$ is the DSC lattice spacing. The magnitude of the Burgers vector DD′ associated with this step is $S = 2d_{DSC}$. For the coupling factor, we immediately obtain $\beta = -S/H = -2/3$. These values of H, S and β match our geometric model of coupling for the ⟨1 1 0⟩ mode (Sections 9.2 and 9.3) and results of MD simulations.

A disconnection corresponding to the ⟨1 0 0⟩ mode of coupling can be obtained by displacing the white crystal to the right by the DSC vector EE′ and terminating this displacement at point E′. The magnitude of the Burgers vector remains the same ($S = 2d_{DSC}$) but the step height becomes $H = 2d_{DSC}$, resulting in $\beta = 1$. These values of H, S and β are again consistent with our geometric model for the ⟨1 0 0⟩ mode.

Coupling characteristics of all other GBs, with both low- and high-angle misorientations, can be also expressed in terms of suitable DSC vectors. The two branches of β arise in this analysis from choosing shifts of the white lattice either to the right or to the left.

We emphasize that this analysis in purely geometric and its capability to predict the disconnection properties and thus β is limited. In the example shown in Fig. 23, the grain translations DD′ and EE′ were correctly selected out of many possible choices because they gave the smallest magnitudes of H and/or S. But these are not well-defined or physically justified criteria. They are not followed in all cases, as shown by the examples in Fig. 11. The actually observed disconnection step vector (H, S) is the one which gives the lowest critical resolved stress. It can only be established by atomistic modeling or experiment. The utility of this geometric analysis is in its ability to identify a few DSC vectors which are reasonable candidates for the actual step vector. This can be readily done for both low- and high-angle GBs.

10. Critical stresses for boundary motion

Within the dislocation model, the critical stress for GB motion at low temperatures is related to the Peierls–Nabarro stress for the GB dislocation glide. Qualitatively, Peierls–Nabarro stresses of different dislocations can be compared by examining sections of gamma surfaces corresponding to relevant slip planes and slip directions. A gamma surface represents the excess energy function $\gamma(\mathbf{t})$ of a generalized stacking fault obtained by relative translation of two half-crystals by a vector $\mathbf{t}$ parallel to a chosen crystallographic plane [53]. This energy is calculated by allowing atomic relaxations normal to the fault plane but

prohibiting atomic movements in parallel directions. Burgers vectors of perfect dislocations correspond to translation vectors **t** connecting nearby global minima on the gamma surface. The energy $\gamma(t)$ along a Burgers vector, together with the relevant elastic constants, provide input to the Peierls–Nabarro model of a planar-core dislocation [54,55]. A higher energy barrier on $\gamma(t)$ leads to a more compact dislocation core and thus a larger Peierls–Nabarro stress.

Applying this approach, the gamma surfaces shown in Fig. 24 indicate that the $\{100\}\langle 100\rangle$ slip responsible for the $\langle 100\rangle$ mode of coupling must be much more difficult than the $\{110\}\langle 110\rangle$ slip corresponding to the $\langle 110\rangle$ mode. As was established by the MD simulations (Section 7), the [100] dislocations behave as if dissociated in the (010) slip plane in two $1/2\langle 110\rangle$ dislocations according to the reaction (6). They glide by a vector $1/2\langle 110\rangle$ at a time. This slip behavior can now be understood by noting that the energy maximum on the gamma surface for the $\{100\}\langle 110\rangle$ slip is much lower than for the purely cubic $\{100\}\langle 100\rangle$ slip.

Furthermore, the $\{100\}\langle 110\rangle$ energy maximum is still higher than for the $\{110\}\langle 110\rangle$ slip. This suggests that the critical resolved shear stress required for activating the $\langle 100\rangle$ mode of coupling must be larger than for the $\langle 110\rangle$ mode. Of course, this prediction should be taken with caution since the slip of [100] dislocations involves complex atomic movements in both the edge and screw directions and may not closely follow the one-dimensional Peierls–Nabarro model. In addition, elastic interactions between the GB dislocations can modify the Peierls–Nabarro stress relative to that for an isolated dislocation. Nevertheless, the prediction of the relative easiness of the $\langle 110\rangle$ coupling mode is consistent with the observation that the switch between the modes occurs at $\theta < 45°$ (Fig. 7).

Note that pre-existing GB disconnections and other extrinsic defects, as well as various stress concentrators in the material, can significantly reduce the critical stress of coupled GB motion.

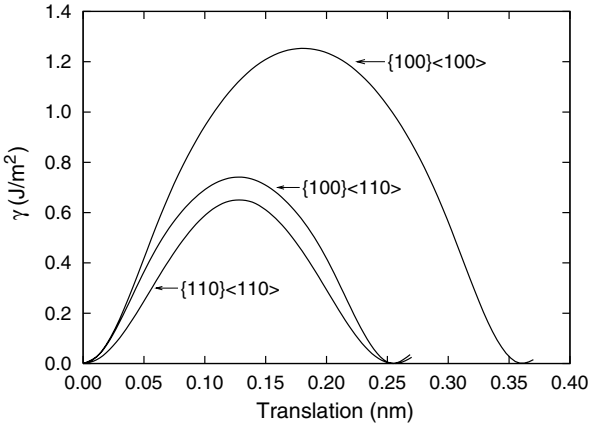

Fig. 24. Sections of gamma surfaces of Cu calculated with the embedded-atom potential used in this work, showing that the $\{100\}\langle 100\rangle$ slip for low-angle GB motion is very difficult.

11. Discussion and outlook

11.1. Summary

That shear stresses can trigger the motion of high-angle GBs, and that conversely, the volume swept by a GB undergoes a shear β, has been found only recently [3–5]. Our atomistic simulations of this coupled GB motion show that both effects occur and follow our geometric predictions with high accuracy for all misorientation angles θ at temperatures below $\sim 0.7T_m$ and for most low-angle GBs at almost all temperatures. Our geometric model of coupling predicts that, in the range $0 < \theta < 90°$ for a positive shear stress, there is a positive and a negative branch (mode) of coupling, on which the GB dislocation content **B**, the coupling factor β and the normal GB velocity v_n are all, respectively, positive and negative. Each branch connects smoothly, and without change of sign, to the respective low-angle limit where individual GB dislocations are resolved. We find the dislocation Burgers vector $\mathbf{b} = \langle 100\rangle$ and $\beta \approx \theta$ when θ is small, and $\mathbf{b} = -(1/2)\langle 110\rangle$ and $\beta \approx -(\pi/2 - \theta)$ when θ approaches 90°.

Our simulations of copper GBs reveal an abrupt transition between the positive and negative branches of coupling at $\theta \approx 35°$ for temperatures between 500 and 800 K. At lower temperatures, the negative $\langle 110\rangle$ branch continues to very small θ values. There is a range of temperatures and angles, where dual behavior is seen: GB motion begins with negative behavior and is replaced by positive after a short time. All boundaries studied are able to move in either mode of coupling. The selection of the mode depends on the critical stresses and Schmid factors, as well as on symmetry-breaking imperfections in the GB structure.

The details of atomic movements in the two modes of coupling have been studied and the mechanism of motion has been found for each mode. All GBs move by deformation of their structural units, accompanied by relatively small and highly correlated (“military”) displacements of the atomic sites. During the passage of the GB, atoms can diffuse but must eventually settle on geometrically prescribed sites once the GB has passed. Thus, perfect coupling does not require diffusion, but diffusion can occur without affecting perfect coupling.

In the low-angle regimes of the two coupling modes, the correlated atomic movements are localized in the neighborhood of the dislocation cores and represent atomic mechanisms of dislocation glide. When θ is near 90°, the low-temperature stress required to move the GB approaches the Peierls–Nabarro stress of the usual $-1/2[110]$ dislocations gliding on unusual $(1\bar{1}0)$ slip plane. As θ decreases, interactions between the dislocations change this stress and make it a function of θ that is sensitive to whether the GB is flat or zigzag.

At high temperatures, coupled motion of high-angle GBs begins to be interrupted by individual sliding events, whose frequency grows with temperature. The mechanism

of the sliding events can be associated with stress-induced GB premelting. In our simulations, the stress drops after each sliding event and the GB resolidifies. The next event can be coupling in one of the modes or sliding. The existence of this crossover regime at high temperatures clearly indicates that coupling and sliding can coexist in the same boundary. As the temperature is increased further, coupling disappears and the GB response to shear changes entirely to rigid sliding. Low-angle GBs remain coupled up to almost the melting point. The diagram of mechanical responses of the GBs (Fig. 8) shows domains of coupling, sliding and dual behavior in the temperature–angle coordinates. We suggest that such diagrams can be useful for the interpretation and prediction of mechanical behavior of GBs.

The coupling provides a low-temperature, stress-induced mechanism for GB motion and for additional plasticity of the material down to 0 K. GB sliding is another plasticity mechanism, which replaces coupled GB motion at high temperatures.

11.2. Implications of this work

GB and heterophase-interface motion are part of many processes in materials, including grain growth, recrystallization, plasticity, phase transformations and diffusion-induced GB migration (DIGM) [56]. The discovery of the coupling effect suggests a need for a major re-examination of our understanding of these and many other phenomena in materials science, in which coupled interface motion might play a significant role. Such phenomena include the following:

1. It was thought for a long time that motion of high-angle GBs occurs by random diffusive jumps of atoms across the GB [57]. The only known exception was the motion of twin boundaries, which produces shear deformation and does not involve any diffusion. Our work amends this picture in two ways. Firstly, there is a large class of high-angle GBs that can move in a coupled manner similar to twin boundaries. Secondly, we have shown that diffusion and coupled GB motion do not exclude each other.
2. Grain rotation is a likely result of coupled motion of curved interfaces. This effect was studied in simulations of included grains [3,6], but the process becomes more complicated when the grain is bounded by junctions of GBs.
3. As grains grow, the coupling will produce inhomogeneous shear deformation, incompatibilities and stresses which can affect the kinetics and morphology of grain growth. Grain growth should produce upheavals on the free surface which are different from thermal grooving.
4. The $6 - n$ "law" of grain growth in two dimensions [58] is derived by assuming motion by curvature and $\pi/3$ corners. The parabolic "law" of grain growth is derived from self-similarity and scaling. Both "laws" assume uniform isotropic GBs and thus are rarely expected to hold in experiment. Coupling should lead to additional deviations from these "laws".
5. Recrystallization on heating after cold deformation is probably triggered by the existence of dislocation-free volumes swept by coupled GB motion during later stages of the cold work. Such volumes are able to grow without a nucleation barrier at high temperatures, driven by the stored cold work in their surroundings. The textures found in many recrystallized structures may originate from the dislocation-free volumes formed along cold-worked GBs moved by coupling.
6. Dynamic recrystallization occurs during high-temperature deformation. The current understanding of this process is based on apparent continual nucleation of new grains, their growth and subsequent deformation. This view may change if coupled GB motion induced by the deformation leads to a continual formation of volumes large enough to continue to grow. Grain rotation can contribute an additional driving force for the GB motion.
7. Stress-induced GB migration can produce grain shape changes and rotation, and thus plastic deformation of polycrystalline materials without diffusion or slip in the grains. This is another deformation mechanism, besides diffusional creep and slip, which is characterized by a different grain-size and temperature dependencies of the deformation rate. This mechanism is especially important in deformation behavior of nanocrystalline materials.
8. Stress-induced GB displacements have been found to trigger grain growth during tensile tests at room temperature [26,27] and the more extensive grain growth at cryogenic temperatures than at room temperature during indentation creep tests of nanostructured materials [28].
9. The moving GBs in DIGM and discontinuous precipitation are thought to be driven by strains from compositional inhomogeneities. The nucleation during these processes has long been a mystery. It too could be triggered by coupling to the coherency stress. This could be verified by studying the effect of applied stresses on these processes.
10. Coupled motion of interfaces can occur during phase transformations The well-known example is offered by martensitic transformations, in which there is a geometric relation between the phases and a habit plane derivable from the transformation shear. Closely related is another class of transformations, which are controlled by long-range diffusion but display a morphology of shear transformations. This coexistence of shear and diffusion was the subject of a long-standing polemic in the literature [59,60]. The new phase grows in the form of plates with a strict orientation relationship and a habit plane derivable from martensite theory. But, because the new phase is required by thermodynamics

to have a chemical composition different from the matrix composition, long-range diffusion must occur [61]. This process has a certain similarity with coupled GB motion, which we have found to coexist with diffusion (Section 4). It is the lattice that is sheared during both processes, while individual atoms can diffuse between the lattice sites.

This list could be continued to other topics, such as deformation of thin films and nanowires, superplasticity, etc.

11.3. Existing challenges and future work

Planar grain boundaries are characterized by five angles and the direction of the shear in the GB plane, which adds another angle. We have explored this six-dimensional configuration space by studying only a set of [0 0 1] symmetrical tilt GBs with the shear applied in the direction normal to the tilt axis. These GBs sample a trajectory in this space on which five angles are fixed and only the tilt angle θ is varied. We intend to explore other simple one- or two-angle trajectories: changing the tilt axis to produce other sets of CSLs, varying the GB plane to produce asymmetrical tilt boundaries or to follow a trajectory from tilt to twist GBs, or rotating the direction of $v_{\|}$. Preliminary simulations reveal that asymmetrical tilt GBs do couple with shear stresses and produce shear deformation of the lattice. This work would greatly benefit from concurrent experimental measurements of coupling in precisely oriented bicrystals [62]. The geometric model of coupling introduced in Section 9.3 must be extended to general angles and its predictions tested by MD simulations.

Because GBs have atomic structure and are usually not isotropic about their normals, coupling should be a general phenomenon, but it is forbidden for special symmetries of the GBs and of the shear direction. For example, coupling should not be seen for pure twist GBs or for a strain applied parallel to the tilt axis. All such symmetries can be formulated as specific equations among the angles. One such equation defines a hypersurface in the six-dimensional space, several equations define lower-dimensional features, but all of them together occupy a very small portion of this space, specifically with no six-dimensional volume. Thus, almost every "general" point in the six-dimensional space represents a GB that can move by coupling, including the points representing the symmetric tilt CSL GBs that we have studied, which are often called "special" by a different criterion.

Junctions of GBs provide another complication for coupling, easily seen for small-angle GBs. While the dislocations in the GB of an included grain are conserved and increase in density as the grain shrinks [6], those in the GBs bounding a grain with more than one neighbor can leak from one GB into another at the triple junctions. Formulating this complication is a formidable task, with considerable history in the study of polygonization [63]. There is also a problem of compatibility among coupled movements of GBs meeting at multiple junctions.

We cannot describe our results by the concept of GB mobility [57]. The dynamics of coupled GB motion can be diverse, ranging from stick–slip behavior to stochastic motion. In our simulations the stress continues to rise until the GB yields. At 0 K, the GB moves only when a critical stress is reached. As the temperature increases, the peak stress is reduced, presumably by several quite different, thermally activated mechanisms, which need to be studied. Our simulations show that at relatively high temperatures with the free boundary condition, GB motion is stochastic with zero average velocity. The effect of a very small $v_{\|}$ (down to 10^{-4} m/s) imposed by the fixed boundary condition is currently being studied. It is expected that such small velocities should impose a net normal GB motion without changing its stochastic character. In this limit, a linear relation between the average v_n and stress is expected and the concept of mobility will be plausible.

Our simulation geometry is that of a soft machine, in which a large amount of strain is accumulated in the grains and is reduced by S/L at each step of the grain translation S along the GB, where L is the grain size in the normal direction. This results in the saw-tooth behavior of the stress. This behavior should be observable experimentally, although it becomes too small if L is large. It manifests itself in a stop–go (jerky) GB motion, sometimes seen in experiments, including in situ high-resolution electron microscopy observations [38]. The stick–slip behavior is very similar to sliding friction [39,40]. Some of the ideas and models developed in that area should be adapted for describing the temperature dependence of the velocity–stress relations for GBs.

We have demonstrated that coupling ceases to exist at high temperatures for our high-angle tilt GBs. The transition from coupling to sliding seems to occur by stress-assisted melting fluctuations at the GB at temperatures below the GB premelting temperature without stress. Such fluctuations were introduced by Frenkel [64] and postulated as the activated process in GB motion by Mott [65]. We believe that the increase in the GB free energy caused by the stress facilitates such fluctuations. A liquid region slides easily, which puts more mechanical load on the unmelted portion of the boundary. This load, in turn, increases the probability of premelting in other regions and they also begin to slide. As a result, the sliding quickly propagates over a large GB area until the stress drops and the premelted regions resolidify.

The multiplicity of coupling modes endows high-angle GBs with much flexibility in responding to applied stresses or other driving forces. This flexibility is important for many processes involving GB motion, in particular for accommodating the incompatibility in the movements of adjacent GBs or parts of a curved one [66]. Consider a process in which a GB moves up and down by switching between one mode with $\beta_1 > 0$ and another with $\beta_2 < 0$.

If the grains are forced to translate relative to each other with a velocity $v_{\parallel} > 0$, the GB velocity can switch back and forth between $v_{n1} = v_{\parallel}/\beta_1 > 0$ and $v_{n2} = v_{\parallel}/\beta_2 < 0$. The durations of the two modes can be adjusted to give any average between v_{n1} and v_{n2}, including $\langle v_n \rangle = 0$, for which the boundary will appear to be stationary and the process will look like GB sliding. As indicated in Fig. 8, switches between coupling modes are most probable at high misorientation angles; low-angle boundaries are unlikely to "slide" by this mechanism. Although it is conceptually plausible, some evidence for this mechanism has only been obtained in the range of dual behavior (Fig. 10).

Note that coupled GB motion can also occur without producing net shear deformation of the bulk. Suppose a driving force induces normal GB motion with a constant velocity $v_n > 0$. If this motion is coupled but there are constraints imposed on grain translations, the GB can move by switching back and forth between two modes. The lattice regions adjacent to the boundary will then experience relative translations with alternate velocities $v_{\parallel 1} = \beta_1 v_n > 0$ and $v_{\parallel 2} = \beta_2 v_n < 0$. The switching times between the modes can be adjusted to give a range of $\langle v_{\parallel} \rangle$ values, including $\langle v_{\parallel} \rangle = 0$.

In conclusion, we believe that the consideration of the coupling effect might lead to solution of many long-standing puzzles, and offer new and deeper understanding of the complexity of GBs.

Acknowledgements

We appreciate the constructive criticism by U.F. Kocks. This work was supported by the US Department of Energy (Office of Basic Energy Sciences, Division of Materials Sciences) under contract DE-FG02-01ER45871-0006.

Appendix A

To derive the relation

$$\mathbf{R}\hat{\mathbf{g}} - \hat{\mathbf{g}} = B\hat{\mathbf{p}} \tag{25}$$

appearing in Section 9.3 we first use Eq. (19) with **B** substituted from Eq. (18). We have

$$\mathbf{X} \equiv \mathbf{RB} - \mathbf{B} = \hat{\mathbf{p}} - \mathbf{R}\hat{\mathbf{p}} - (\mathbf{R}^{-1}\hat{\mathbf{p}} - \hat{\mathbf{p}}) = 2\hat{\mathbf{p}} - \mathbf{R}\hat{\mathbf{p}} - \mathbf{R}^{-1}\hat{\mathbf{p}}.$$

Since the second and third terms in the right-hand side of this equation are obtained by rotations of $\hat{\mathbf{p}}$ in opposite directions, **X** is parallel to $\hat{\mathbf{p}}$. Therefore, the length of vector **X** equals

$$X = \mathbf{X}\hat{\mathbf{p}} = (2\hat{\mathbf{p}} - \mathbf{R}\hat{\mathbf{p}} - \mathbf{R}^{-1}\hat{\mathbf{p}})\hat{\mathbf{p}} = 2\hat{\mathbf{p}}(\hat{\mathbf{p}} - \mathbf{R}^{-1}\hat{\mathbf{p}}), \tag{26}$$

where we used the fact that $(\mathbf{R}\hat{\mathbf{p}})\hat{\mathbf{p}} = (\mathbf{R}^{-1}\hat{\mathbf{p}})\hat{\mathbf{p}}$ (vectors obtained by opposite rotations of $\hat{\mathbf{p}}$ have identical projections on $\hat{\mathbf{p}}$). Using Eq. (18) we can rewrite (26) as

$$X = -2\mathbf{B}\hat{\mathbf{p}}. \tag{27}$$

On the other hand, since rotations preserve length, we have $(\mathbf{R}^{-1}\hat{\mathbf{p}})(\mathbf{R}^{-1}\hat{\mathbf{p}}) = 1$, or by Eq. (18),

$$(\mathbf{B} + \hat{\mathbf{p}})^2 = B^2 + 2\mathbf{B}\hat{\mathbf{p}} + 1 = 1$$

and thus

$$B^2 = -2\mathbf{B}\hat{\mathbf{p}}. \tag{28}$$

Comparing Eqs. (27) and (28) we conclude that $X = B^2$, or multiplying this relation by $\hat{\mathbf{p}}$,

$$X\hat{\mathbf{p}} = \mathbf{X} = \mathbf{RB} - \mathbf{B} = B^2\hat{\mathbf{p}}.$$

Finally, dividing the latter relation by B we arrive at Eq. (25) with $\hat{\mathbf{g}} \equiv \mathbf{B}/B$.

References

[1] Sutton AP, Balluffi RW. Interfaces in crystalline materials. Oxford: Clarendon Press; 1995.
[2] Balluffi RW, Allen SM, Carter WC. Kinetics of materials. Hoboken (NJ): John Wiley and Sons; 2005.
[3] Cahn JW, Taylor JE. Acta Mater 2004;52:4887.
[4] Suzuki A, Mishin Y. Mater Sci Forum 2005;502:157.
[5] Cahn JW, Mishin Y, Suzuki A. Philos Mag 2006;86:3965.
[6] Taylor JE, Cahn JW. Acta Mater, in press.
[7] Li CH, Edwards EH, Washburn J, Parker J. Acta Metall 1953;1:223.
[8] Bainbridge DW, Li CH, Edwards EH. Acta Metall 1954;2:322.
[9] Kittel C. Introduction to sold state physics. New York (NY): Wiley-Interscience; 1986.
[10] Biscondi M, Goux C. Mem Sci Rev Met 1968;75:167.
[11] Fukutomi H, Iseki T, Endo T, Kamijo T. Acta Mater 1991;39:1445.
[12] Winning M, Gottstein G, Shvindlerman LS. Acta Mater 2001;49:211.
[13] Winning M, Gottstein G, Shvindlerman LS. Acta Mater 2002;50:353.
[14] Winning M, Rollett AD. Acta Mater 2005;53:2901.
[15] Sheikh-Ali AD, Szpunar JA, Garmestani H. Interface Sci 2003;11:439.
[16] Yoshida H, Yokoyama K, Shibata N, Sakuma YIAT. Acta Mater 2004;52:2349.
[17] Molteni C, Francis GP, Payne MC, Heine V. Phys Rev Lett 1996;76:1284.
[18] Molteni C, Marzari N, Payne MC, Heine V. Phys Rev Lett 1997;79:869.
[19] Hamilton JC, Foiles SM. Phys Rev B 2002;65:064104.
[20] Chen LQ, Kalonji G. Philos Mag A 1992;66:11.
[21] Shiga M, Shinoda W. Phys Rev B 2004;70:054102.
[22] Chandra N, Dang P. J Mater Sci 1999;34:655.
[23] Haslam AJ, Moldovan D, Yamakov V, Wolf D, Phillpot SR, Gleiter H. Acta Mater 2003;51:2097.
[24] Sansoz F, Molinari JF. Acta Mater 2005;53:1931.
[25] Shan Z, Stach EA, Wiezorek JMK, Knapp JA, Follstaedt DM, Mao SX. Science 2004;305:654.
[26] Jin M, Minor M, Morris JW. J Mater Res 2005;20:1735.
[27] Gianola DS, Van Petegem S, Legros M, Brandstetter S, Van Swygenhoven H, Hemker KJ. Acta Mater 2006;54:2253.
[28] Zhang K, Weertman JR, Eastman JA. Appl Phys Lett 2005;87:061921.
[29] Upmanyu M, Smith RW, Srolovitz DJ. Interface Sci 1998;6:41.
[30] Upmanyu M, Srolovitz DJ, Lobkovsky AE, Warren JA, Carter WC. Acta Mater 2006;54:1707.
[31] Srinivasan SG, Cahn JW. In: Ankem S, Pande CS, Ovidko I, Ranganathan R, editors. Science and technology of interfaces. Seattle (WA): TMS; 2002. p. 3–14.
[32] Read WT, Shockley W. Phys Rev 1950;78:275.
[33] Mishin Y, Mehl MJ, Papaconstantopoulos DA, Voter AF, Kress JD. Phys Rev B 2001;63:224106.
[34] Suzuki A, Mishin Y. Interface Sci 2003;11:131.
[35] Lutsko JF, Wolf D, Phillpot SR, Yip S. Phys Rev B 1989;40:2841.
[36] Hirth JP, Lothe J. Theory of dislocations. 2nd ed. New York (NY): Wiley; 1982.

[37] Sutton AP, Vitek V. Philos Trans Roy Soc Lond A 1983;309:1.
[38] Merkle KL, Thompson LJ, Phillips F. Interface Sci 2004;12:277.
[39] Persson BNJ. Sliding friction. Physical properties and applications. 2nd ed. Berlin: Springer; 2000.
[40] Reimann P, Evstigneev M. New J. Phys. 2005;7:1.
[41] Suzuki A, Mishin Y. J Mater Sci 2005;40:3155.
[42] Hirth JP. J Phys Chem Solids 1994;55:985.
[43] Hirth JP, Pond RC. Acta Mater 1996;44:4749.
[44] Pond RC, Celotto S. Int Mater Rev 2003;48:225.
[45] Christian JW, Crocker AG. In: Nabarro FRN, Duesbery MS, editors. Dislocations in solids, vol. 10. Amsterdam: Elsevier/North-Holland; 1980. p. 165–249.
[46] Christian JW. The theory of transformations in metals and alloys. Oxford: Elsevier; 2002.
[47] Frank FC. In: Symposium on the plastic deformation of crystalline solids. Pittsburgh (PA): Office of Naval Research; 1950. p. 150.
[48] Bilby BA. In: Bristol conference report on defects in crystalline materials. London: Physical Society; 1955. p. 123.
[49] Bilby BA. In: Sneddon IN, Hill RP, editors. Progress in solid mechanics, vol. 1. p. 330–98.
[50] Bullough R, Bilby BA. Proc Phys Soc B 1956;69:1276.
[51] Read WT. Dislocations in crystals. New York (NY): McGraw-Hill; 1953.
[52] King AH, Smith DA. Acta Crystallogr A 1980;36:335.
[53] Vitek V. Crystal Lattice Defects 1974;5:1.
[54] Nabarro FRN. Proc Phys Soc 1947;59:256.
[55] Nabarro FRN. Theory of crystal dislocations. New York (NY): D-over; 1987.
[56] King AH. Int Mater Revs 1987;32:173.
[57] Gottstein G, Shvindlerman LS. Grain boundary migration in metals. Bota Raton (FL): CRC Press; 1999.
[58] Mullins WW. J Appl Phys 1957;28:333.
[59] Aaronson H, Reynolds WT. Scripta Metall 1988;22:567; Aaronson H, Reynolds WT. Scripta Metall 1988;22:575.
[60] Christian JW, Edmonds DV. Scripta Metall 1988;22:573; Christian JW, Edmonds DV. Scripta Metall 1988;22:577.
[61] Aaronson HI, Hirth JP, Rath BB, Wayman CM. In: Pacific rim conference on the roles of shear and diffusion in the formation of plate-shaped transformation products, Kona, Hawaii December 18–22, 1992; Proceedings published in Metall Mater Trans A, 1994;25.
[62] Molodov DA, Ivanov VI, Gottstein G. Acta Mater, in press.
[63] Hibbard WA, Dunn CG. Creep and recovery. Metals Park (OH): ASM; 1957.
[64] Frenkel J. Kinetic theory of liquids. New York: Dover; 1955.
[65] Mott NF. Proc Phys Soc 1948;60:391.
[66] Taylor JE. in press.